L. L. Rutger

EG&G
MOUND APPLIED TECHNOLOGIES

High Temperature Compatibility of 60-Watt IHS Materials

Produced For
EG&G Mound Applied Technologies

By
C. M. Worley and C. W. Merten
Mound Engineering & Analysis Group, Inc.

November 21, 1995

MOUND
is operated for the
U. S. Department of Energy
under contract No. DE-AC04-88-DP43495

DISCLAIMER

High Temperature Compatibility of 60-Watt IHS Materials

Produced For
EG&G Mound Applied Technologies

By
C. M. Worley and C. W. Merten
Mound Engineering & Analysis Group, Inc.
November 21, 1995

I. Introduction

The 60-Watt Isotopic Heat Source (IHS) utilizes a variety of materials which have been selected for their properties at elevated temperatures. These include iridium, molybdenum, and the T-111 alloy which consists of 90 wt% tantalum, 8 wt% tungsten, and 2 wt% hafnium. Properties of interest in radioisotopic heat source applications include high temperature strength, resistance to oxidation, weldability, and ability to act as a diffusion barrier. Iridium is utilized as a clad for fuel pellets because of its high temperature mechanical properties and good compatibility with carbon and plutonium oxide. Molybdenum retains good high temperature strength and has been used as a diffusion barrier in past applications. However, molybdenum also exhibits poor resistance to oxidation. Therefore, it is necessary to enclose molybdenum components so that they are not exposed to the atmosphere. T-111 exhibits moderate oxidation resistance, good high temperature mechanical properties, and good weldability. For these reasons, it is used as the outer containment boundary for the 60-Watt IHS.

Because the temperature in GPHS fueled clads is on the order of 1000 degrees Celsius in the 60-W configuration, the potential for diffusion of dissimilar materials from one into another exists. Deleterious effects of diffusion can include degradation of mechanical strength through the formation of brittle intermetallics, degradation of mechanical properties through simple alloying, or formation of voids through the Kirkendall effect. Because of the possibility of these effects, design methodology calls for use of diffusion barriers between materials likely to exhibit interdiffusion at elevated temperatures. The necessity to assure the long term integrity of the 60-Watt IHS dictates that the diffusion behavior of its component materials be known. This report describes the high temperature compatibility studies which were conducted on the component materials of the 60-Watt IHS.

II. Conditioning of Diffusion Couples

Diffusion couples selected for investigation were T-111/molybdenum, molybdenum/iridium, and iridium - T-111. Coupons of each material were approximately 12.7 mm in diameter. T-111 coupons were 5.1 mm thick, molybdenum coupons 0.66 mm thick, and iridium coupons 0.41 mm thick. Before assembly, the faces of each coupon were ground to a 1000 grit finish in an attempt to assure good contact. Coupons were press fit into tantalum - 10% tungsten cans so that one iridium and one molybdenum coupon were sandwiched between T-111 coupons situated at either end of a given can. The T-111 coupon at the open end of the can was first tack welded to maintain contact between coupon faces. Subsequent electron beam welding was performed to provide a means of maintaining contact between coupons which was more resistant to separation through thermal expansion. Tantalum - 10 % tungsten cans containing coupons were then welded into Hastelloy S cans in an argon atmosphere. Secondary containment of the diffusion couples in this manner assured that at worst, the couples would be exposed only to an argon atmosphere and that they would not be exposed to oxygen at elevated temperatures. The presence of oxygen at elevated temperatures could confound results through simple oxidation or vapor phase transport of molybdenum oxide as noted by Ohriner and George (1991).

Twelve samples were prepared for conditioning in accordance with the times and temperatures given in the matrix presented in Table 1. Times and temperatures were selected on the basis of previous studies which were conducted with similar alloys. Three conditioning times were associated with each of four conditioning temperatures. After thermal conditioning, each sample was metallographically prepared for examination of its three diffusion couples.

III. Theory

In ideal cases, the behavior of diffusion couples as a function of time and temperature may be predicted. Specifically, the concentration of a solid solute in a solid solvent at a given distance from the initial interface between the solute and solvent as a function of time can be deduced from Fick's Second Law. For cases where diffusivity, D, is independent of concentration,

$$\frac{dC_x}{dt} = D\frac{d^2C_x}{dx^2} \tag{1}$$

where C_x is the concentration of diffusing species or solute, t is time, D is diffusivity, and x is the distance between the initial solute/solvent interface. For boundary conditions given by $C = C_o$ at $t = 0$ for $0 < x < \infty$ and $C = C_s$ at $x = 0$ for $0 < t < \infty$, the solution to equation 1 is given by

$$\frac{C_x - C_o}{C_s - C_o} = 1 - \varphi\left(\frac{x}{2\sqrt{Dt}}\right) \tag{2}$$

where φ is the Gaussian Error Function. For wavelength dispersive x-ray analysis, the detection threshold is assumed to be one percent. Then the concentration, C_x, which corresponds to the detectable limit of the extent of diffusion is 0.01. The initial concentration of the solute in the solvent, C_o, is 0.00. The concentration of the solute at the interface, C_s, is assumed to be 1.00. Substitution of values for concentration into equation 2 gives

$$0.99 = \varphi\left(\frac{x}{2\sqrt{Dt}}\right). \tag{3}$$

Evaluation of the Gaussian Error Function shows that when $\varphi(y) = 0.99$, the argument, y, is equal to 1.820. Therefore,

$$x = 3.640\sqrt{Dt} \tag{4}$$

or,

$$x^2 = 13.2496Dt \tag{5}$$

Equation 5 can be used to determine the diffusivity, D, at a given temperature from the time, t, and the distance which the solute or diffusing species has diffused into the solvent. This is done by plotting x^2 against t for various times and fitting a straight line to the data using a least squares regression. The diffusivity is determined from the slope of the line and has units of length^2/time.

Over a range of temperatures, diffusivities obey an Arrhenius relation of the form

$$D = D_o e^{-\frac{Q}{RT}} \tag{6}$$

where Q is an activation energy, D_o is a frequency factor, R is the universal gas constant, and T is the absolute temperature. Equation 6 may be rearranged in the form of a linear equation to give

$$\ln D = \ln D_o - \frac{Q}{R}\left(\frac{1}{T}\right) \tag{7}$$

When the natural logarithm of the diffusivity is plotted against the reciprocal of the absolute temperature, a straight line with a slope of - Q/R and intercept at ln D_o results.

For a given time and temperature, the extent of the diffusion zone may be predicted. Using Q and D_o, which are determined from equation 7 and experimental data for diffusivity D, the theoretical diffusivity for a given temperature may be predicted from equation 6. The concentration of the solute, C_x, for a given time, t, at a given distance, x, from the solute-solvent interface is given by equation 2. The extent of the diffusion zone observable with x-ray microprobe may be predicted for a given time and temperature from equation 4 by substituting time at temperature and theoretical diffusivity. Values for extent of the diffusion zone predicted by equation 4 may also be compared with measured values of diffusion zone thickness to assess the validity of theoretical diffusivities predicted by equation 7.

IV. Evaluation of Diffusion Zones

After thermal conditioning, samples were metallographically prepared for analysis by electron microprobe. First, tantalum - 10% tungsten cans were removed from Hastelloy S cans and potted in epoxy. The epoxy mounts were then each cut to reveal an axial plane close to the central axis of the sample. After cutting, samples were remounted in epoxy in order to fill any voids present within the tantalum - 10% tungsten can. Preparation of surfaces began with grinding using silicon carbide paper through 600 grit. Samples were then hand lapped on Texmet cloth with 15 μm diamond paste followed by hand lapping with 9 μm diamond paste. Hand lapping was followed by a vibratory polish using 6 μm diamond for 24 hours, and then 1 μm diamond for 24 hours.

Diffusion zones on specimens were evaluated using a variety of electron microprobe techniques. Both secondary and backscattered electrons were used to image the interfaces of diffusion couples. Backscattered electrons are sensitive to atomic number. Through adjustments in probe current, it is possible to resolve fractional differences in atomic number such as those due to alloying, or to image differences in grain orientation. Secondary electrons are useful in imaging topography and are used in microprobe analysis of diffusion couples to detect features such as separations at interfaces. Characteristic x-rays, emitted by elements present in a specimen, can be detected in a variety of ways to yield useful information. Because they offer better resolution than energy dispersive x-ray spectrometers, wavelength dispersive spectrometers were used to detect characteristic x-rays. As an electron beam is scanned across a specimen, a two dimensional spatial map of x-rays emitted within a bandwidth centered about a characteristic wavelength can be created. The corresponding image is displayed as a series of white dots on a black background and is known as an x-ray dot map. Simultaneous use of a number of spectrometers set for appropriate wavelengths allows quantitative analysis to be performed on a small volume of material. Typically, the diameter of the volume on which such an analysis can be performed is on the order of one μm. By stepping the electron beam in a line across a specimen, a number of quantitative analyses can be performed in succession. A plot of the results of these quantitative analyses versus distance from the location of the first analysis is known as a line scan profile.

A secondary electron image, three backscattered electron images, molybdenum x-ray dot map, and iridium x-ray dot map of a molybdenum - iridium diffusion couple are shown in Figures 1 - 6. In analyzing this diffusion couple, x-ray dot maps were first used in an attempt to establish the locations of each element with respect to the original interface. The molybdenum x-ray dot map in Figure 5 shows at least four distinct zones, as does the iridium x-ray map shown in Figure 6. Comparison of the molybdenum and iridium x-ray dot maps suggests that the zone at the far left is 100 percent molybdenum, that the zone at the far right is 100 percent iridium, and that the two zones in the middle contain a mixture of molybdenum and iridium. Because the second zone from the left appears to be richer in molybdenum than iridium and because the second zone from the right appears to be richer in iridium than molybdenum, it is assumed that the original molybdenum

- iridium interface was located at the interface of these two zones. X-ray dot maps were then compared with backscattered and secondary electron images in order to determine which microstructural features were associated with which elements. The secondary electron micrograph shown in Figure 1 coupled with information from x-ray dot maps suggests the presence of only two zones where molybdenum and iridium coexist. Backscattered electron micrographs in Figures 2, 3, and 4 show the situation to be more complex. Because of the difference in atomic number between molybdenum and iridium, it is not possible to image all areas of interest simultaneously while maintaining sufficient contrast to detect subtle differences within zones. Figure 2 is a backscattered electron image of the zone which was determined from x-ray dot maps to be 100 percent molybdenum. The backscattered electron image in Figure 3 shows the zone to the left of the original molybdenum - iridium interface which is thought to be richer in molybdenum than iridium. Figure 4 shows all zones to the right of the original molybdenum - iridium interface. Instead of the two zones suggested by x-ray dot maps, there are apparently three. Because they afford the greatest atomic number resolution, backscattered electron images are used for measurement of diffusion zone thickness.

Iridium - T-111 interfaces were analyzed in much the same way as molybdenum - iridium interfaces. Figures 7 through 10 are images of an iridium - T-111 interface produced using techniques described above. Figure 9, an iridium x-ray dot map, shows the existence of at least four zones. Comparison of Figure 10, a tantalum x-ray dot map, with Figure 9 suggests that four zones may also be present in Figure 9. The zone furthest to the left consists of 100 percent iridium and the zone furthest to the right consists of 100 percent T-111. Assuming that only four zones are present, one judges from the x-ray dot maps that the original iridium - T-111 interface was located between the second zone from the left and the second zone from the right. The backscattered electron image in Figure 8 suggests that as many as four zones containing both tantalum and iridium may be present. Three of these zones occupy a narrow band on the T-111 side of the diffusion couple. Initial efforts to determine activation energies and diffusion coefficients for iridium - T-111 diffusion couples were based on the assumption that there are only two distinct zones in which iridium and tantalum coexist. In the diffusion couple shown in Figure 8, the interface between these two idealized zones was assumed to lie between the second zone from the left and the fourth zone from the right.

Secondary electron, backscattered electron, and x-ray dot map images of a T-111 - molybdenum diffusion couple are shown in Figures 11 through 15. Like molybdenum - iridium diffusion couples, the difference in atomic number between tantalum and molybdenum makes it difficult to extend the range of contrast in backscattered electron images sufficiently to image both T-111 and molybdenum. In order to image subtle differences in atomic number with backscattered electrons, it is necessary to image each side of T-111 - molybdenum diffusion couples separately. Examination of the tantalum x-ray dot map shown in Figure 14 and the molybdenum x-ray dot map in Figure 15 indicates that only two zones exist and that molybdenum and tantalum do not coexist in either of these zones.

Diffusion zone thicknesses for molybdenum - iridium and iridium - T-111 diffusion couples were determined from backscattered electron images for each of the time - temperature combinations shown in Table 1. Zone thickness measurements appear in Tables 2 through 5. For a given diffusion couple consisting of materials "A" and "B", measurements associated with the symbology "A>B" indicate the thickness of the diffusion zone in which solute material A has diffused into solvent material B. The original location of the interface between diffusion couple materials was determined as described above. For any given time - temperature pairing, a designation of "NDZ" indicates that no diffusion zone was observed. This is universally the case for all T-111 - molybdenum diffusion couples.

Diffusivities were determined from diffusion zone thickness data using equation 5. For a given diffusion couple, diffusion direction, and temperature, the least squares method was used to fit a straight line to thickness squared versus time data. Diffusivities, y intercepts, and regression coefficients corresponding to each direction of molybdenum - iridium and iridium - T-111 diffusion couples are given in Tables 6 through 9. For completeness, corresponding plots are presented in Appendix 1. Table A1 provides a cross reference between tables and plots. For molybdenum - iridium diffusion couples, a perfect fit is indicated because, in most cases, no more than two data points were observed for any given temperature. Regression coefficients for fit to iridium - T-111 data are generally above 0.96. The exception is the fit to data for diffusion of iridium into T-111 at 1300 degrees Celsius.

For a each diffusion couple and direction, a straight line was fit to diffusivity versus temperature data using equation 7. Resultant frequency factors, activation energies, and regression coefficients are given in Table 10. Corresponding plots from which these parameters were derived are presented in Appendix 1. Inspection shows a good fit to diffusivity versus temperature data for the molybdenum - iridium diffusion couple and a relatively poor fit for the iridium - T-111 diffusion couple. Equation 6 was used to predict diffusivity for each diffusion couple, direction, and temperature. The resulting diffusivities were then used to predict the diffusion zone thicknesses which should have been observed. Predicted diffusion zone thicknesses are compared with observed diffusion zone thicknesses for molybdenum - iridium and iridium - T-111 diffusion couples in Tables 11 through 14. For molybdenum - iridium diffusion couples, predicted and observed diffusion zone thicknesses are in fair agreement. Predicted diffusion zone thickness is generally most accurate for the longest period of time associated with a given temperature. For iridium - T-111 diffusion couples, the agreement between predicted and observed values is extremely poor.

Because the fit to diffusion zone thickness was considered to be unsatisfactory, the nature of iridium - T-111 and molybdenum - iridium diffusion zones was investigated by performing line scans across the interfaces. To increase the spatial resolution of the line scans, sequential analyses were performed at an angle of ten degrees with respect to the plane of the interface. Secondary and backscattered electron micrographs of the region where a linescan was conducted on a iridium - T-111 diffusion couple are shown in Figures 16 and 17. The series of dots which proceed horizontally across Figure 16 are "burn" marks left by the electron beam at the site of each analysis. In performing the quantitative analyses, it was assumed that only tantalum and iridium were present. The effects of tungsten and hafnium were ignored. A plot showing the relative quantities of tantalum and iridium in atomic percent appears in Figure 18. The points on the plot corresponding to 88 percent iridium, 12 percent tantalum correspond to the analysis conducted at what appears to be a discontinuity in the interface in Figure 16. Recalling from an earlier discussion that the possibility for four distinct zones containing both iridium and tantalum exists, it is apparent from Figure 16 that the electron beam spot size is not small enough to sufficiently characterize three of the four possible zones. In the largest of the four zones, the atomic ratio of iridium to tantalum ranges from 3.46:1 to 3.21:1. From Figure 18, one observes that the ratio of iridium to tantalum is relatively constant over this zone. The one analysis conducted in the remaining zones yields a tantalum to iridium ratio of 7.73:1.

In a manner analogous to the iridium - T-111 diffusion couple, a line scan was made across an iridium - molybdenum interface. Secondary and backscattered electron images of the region where the line scan was made appear in Figures 19 and 20. A plot of the relative atomic percentages of molybdenum and iridium appears in Figure 21. From Figures 19 and 20 it is seen that the possibility of three distinct zones which contain both molybdenum and iridium exist. The ratio of molybdenum to iridium in the zone closest to the molybdenum parent metal is relatively constant and ranges from 3.93:1 to 3.52:1. Material which is located in the second of the three possible zones and which borders the first molybdenum rich zone exhibits a molybdenum to iridium atomic percent ratio of 1:1. Although the backscattered electron image in Figure 20 shows the possibility

of a third zone, no clear boundary between the second and third zones is evident in the linescan plot of atomic percentages. Instead it appears that the second and third zones merge smoothly into one another and exhibit characteristics of classical diffusion.

Ohriner and George (1991) studied diffusion couples of iridium and molybdenum. To predict the thickness of intermetallic layers, they used an Arrhenius equation and presumably combined intermetallic layer thicknesses. In an attempt to improve the fit of predicted diffusion zone thickness to observed values in the current study, diffusion zone thicknesses were combined and analyzed using classical diffusion theory. Combined diffusion zone thicknesses for molybdenum - iridium and iridium - T-111 diffusion couples are given in Tables 15 and 16. In each case, combined diffusion zone thickness is the distance from parent metal to parent metal in any given diffusion couple and is equivalent to the sum of the thicknesses of the individual diffusion zones found in any given diffusion couple. Analogous to the methods used to analyze individual diffusion zones, diffusivities for lumped zones were determined using equation 5 and least squares fits to the experimental data. Diffusivities, y intercepts, and regression coefficients for molybdenum - iridium and iridium - T-111 lumped diffusion zones are given in Tables 17 and 18. Plots from which these parameters were derived are presented in Appendix 1. For both types of diffusion couples, all regression coefficients are greater than 0.95. Frequency factors and activation energies were determined by a least squares fit to equation 7. Results are shown in Table 19. For both the molybdenum - iridium and iridium - T-111 diffusion couples, regression coefficients are 0.98 or greater. Values of diffusion coefficients and activation energies in Table 19 were used with equations 6 and 4 to predict total diffusion zone thickness. Predicted total diffusion zone thicknesses are compared to observed total diffusion zone thicknesses in Tables 20 and 21. For molybdenum - iridium diffusion couples, the differences between predicted and observed thicknesses of combined diffusion zones are comparable to the differences between predicted and observed values for zones analyzed separately. In general, predicted values are more accurate for greater time spans. For iridium - T-111 diffusion couples, agreement between predicted and observed values is greatly improved by pooling together of diffusion zones.

V. Discussion

Diffusion was not observed in any of the molybdenum - tantalum interfaces studied. Activation energies and frequency factors for diffusion of molybdenum into tantalum and tantalum into molybdenum are available in the literature. For diffusion of molybdenum into tantalum, the activation energy is 81.0 kcal/mole and the frequency factor is 1.8×10^{-3} cm^2/sec (Borisov et al., 1968). The temperature range over which these values were determined is 1750 - 2220 degrees Celsius. For diffusion of tantalum into molybdenum, the activation energy is 83.0 kcal/mole and the frequency factor is 3.5×10^{-4} cm^2/sec (Borisov et al., 1968). The temperature range over which these values were determined is 1700 - 2150 degrees Celsius. To determine the likelihood of observing diffusion of either of these species into the other, diffusion zone thickness corresponding to one percent concentration of solute was calculated using equation 4. The results are given in Tables 22 and 23. For diffusion of molybdenum into tantalum, the thickness of the diffusion zone for a one percent concentration of molybdenum in tantalum does not exceed 0.27 μm . For diffusion of tantalum into molybdenum, the thickness of the diffusion zone corresponding to a one percent concentration does not exceed 0.09 μm . The results of these calculations are consistent with the failure to observe diffusion at molybdenum - tantalum interfaces in the current study.

Location of original iridium - T-111 interfaces and subsequent curve fitting of thickness data proved troublesome. As described above, a poor fit to the data was achieved when original interface location was determined on the basis of relative concentrations of tantalum and iridium and activation energies and frequency factors were determined for each side of the interface. Photomicrographs appearing in Figures 7, 8, 16, and 17 represent ideal examples of iridium - T-

111 diffusion zones. Although interpretation of micrographs was not hampered by grain boundary diffusion, thickness of iridium - T-111 diffusion zones was far from uniform. Measurements of diffusion zone thickness were based on maximum observed values in well behaved areas of the interface. Voids were commonly observed in iridium - T-111 diffusion zones. A secondary electron image showing typical voids appears in Figure 22. Their presence is most likely due to the Kirkendall effect and suggests that failure to obtain a good fit to diffusion zone thickness may be due to migration of the iridium - T-111 interface. Gaps were also encountered along iridium - T-111 interfaces. Although diffusion zone thickness measurements were not made in the vicinity of gaps, the effect of their existence on the validity of the data was considered. In such cases, samples exhibiting gaps were often reprepared to expose new surfaces for analysis.

Gaps were commonly observed along all interfaces of many of the specimens which were examined. In most cases, evidence of diffusion was not observed on either side of gaps. Lack of diffusion indicates that a gap was present during the high temperature conditioning process and was not a result of metallurgical sample preparation. Lack of evidence of diffusion in the vicinity of a gap indicates that for the interfaces which were studied, intimate contact is required for diffusion to occur. It also indicates the need for positive clamping or use of dead weight to maintain contact of sample interfaces during conditioning.

Attempts to determine separate activation energies and frequency factors for diffusion of tantalum into iridium and diffusion of iridium into T-111 resulted in poor fits to the observed data. When a single activation energy and frequency factor were determined for the entire diffusion zone, the fit to the observed data was much more acceptable. From micrographs and x-ray dot maps of iridium - T-111 interfaces, it is evident that diffusion is occurring in both directions. However, there does not appear to be a sound mathematical basis for assigning one activation energy and frequency factor to a process that is governed by two or more such values. That this practice adequately accounts for thickness of the entire zone as a function of time and temperature is attributed to the fact that all operative materials migration processes are governed by diffusion and that the practice of treating multiple diffusion zones as one produces "averaged" values of activation energy and frequency factor for the entire zone.

In line scans of both iridium - T-111 and molybdenum - iridium diffusion couples, regions of relatively constant composition were observed. In the largest of the iridium - T-111 diffusion zones, the ratio of iridium to tantalum ranged from 3.46:1 to 3.21:1, indicating the presence of a $TaIr_3$ intermetallic. Concentrations of iridium and tantalum as a function of position are shown in Figure 18. Existence of the $TaIr_3$ intermetallic has been confirmed by Knapton (1958) and Dwight and Beck (1959). Molybdenum to iridium ratios of approximately 3.5:1 and 1:1 were observed in a line scan of a molybdenum - iridium diffusion zone as shown in Figure 21. Ohriner and George (1991) report the existence of Ir_3Mo and IrMo intermetallics. The Ir_3Mo intermetallic was not observed in the present study. Raub (1954) reported the existence of a Mo_3Ir intermetallic which coexists with nearly pure molybdenum. It is likely that this is one of the intermetallics observed.

From observations made during the course of this investigation, it is evident that intimate contact between any of the materials studied must be maintained in order for detectable diffusion to occur. Diffusion between iridium and T-111 and between molybdenum and iridium was significant but predictable for temperatures ranging from 1000 to 1400 degrees Celsius. Iridium - T-111 diffusion couples often exhibited Kirkendall voids. Such voids were not observed as frequently in molybdenum - iridium diffusion couples. Evidence of diffusion between molybdenum and T-111 was not observed. From these observations, the following generalizations may be made. Because of the formation of Kirkendall voids, intimate contact between T-111 and iridium should be avoided. Since high temperature contact between molybdenum and T-111 does not produce observable diffusion, molybdenum serves as an effective diffusion barrier for T-111. Although

diffusion between molybdenum and iridium occurs, void formation is not as extensive as that in iridium - T-111 diffusion couples, and the extent of diffusion can be predicted and compensated by design.

In the 60-Watt IHS, the fueled iridium clad is enclosed by a molybdenum liner body and lower support member. The only components in intimate contact with the iridium clad are the molybdenum upper and lower support members. Because their cross sections are relatively thick, degradation of strength as a result of diffusion is not a concern. All components which contact T-111 surfaces are fabricated from either T-111, molybdenum, or Hastelloy S. Because molybdenum serves as an effective diffusion barrier for T-111 and because intimate contact is required for diffusion to occur, degradation of T-111 components by diffusion is not a concern.

V. Conclusions

The diffusion behavior of molybdenum - iridium, iridium - T-111, and molybdenum - T-111 diffusion couples was characterized and quantified. Evidence of diffusion in molybdenum - T-111 diffusion couples was not observed. Measurements taken from molybdenum - iridium and iridium - T-111 diffusion couples were used to determine diffusivities, activation energies, and frequency factors. Diffusion zone thicknesses determined from activation energies and frequency factors were then compared to observed diffusion zone thicknesses. When diffusion zone interfaces and diffusion parameters were established for each side of an interface, the agreement between predicted and observed diffusion zone thickness for molybdenum - iridium diffusion couples was good whereas that for iridium - T-111 diffusion couples was poor. When diffusion parameters were determined on the basis of total diffusion zone thickness, agreement between predicted and observed diffusion zone thicknesses was good for both molybdenum - iridium and iridium - T-111 diffusion couples. In this case, the activation energy for molybdenum - iridium diffusion couples was 77.9 kcal/mole and the frequency factor was 3.03×10^{10} $\mu m^2/hr$. For iridium - T-111 diffusion couples, the activation energy was 77.4 kcal/mole and the frequency factor was 3.84×10^9 $\mu m^2/hr$.

During the course of this study, several intermetallics were observed. The thickest zone in iridium - T-111 diffusion couples consists of $TaIr_3$. Intermetallics observed in molybdenum - iridium diffusion couples include Mo_3Ir and IrMo. Formation of Kirkendall voids is more prevalent in iridium - T-111 diffusion couples than in molybdenum - iridium diffusion couples. As a result, it is recommended that contact between T-111 and iridium be avoided at temperatures in excess of 1000 degrees Celsius for the ten year life of the 60-W heat source.

VI. References

Borisov, E.V., P. L. Gruzin, and S. V. Zemskii, Zashch Pokryt Metal, 2 (1968) p. 104, cited in Weast, R. C., CRC Handbook of Chemistry and Physics, 60th Edition (1973) pp. F-66, F-68.

Dwight, A. E. and P. A. Beck, Trans. AIME, 215 (1959) pp. 976-979, cited in R. P. Elliott, Constitution of Binary Alloys, First Supplement, McGraw-Hill (1965) p. 563.

Knapton, A. G., J. Inst. Metals, 87, 1958-1959, pp. 28-32, cited in R. P. Elliott, Constitution of Binary Alloys, First Supplement, McGraw-Hill (1965) p. 563.

Ohriner, E. K. and E. P. George, "Growth of Intermetallic Layers in the Iridium-Molybdenum System," Journal of Alloys and Compounds, 177 (1991) pp. 219-227.

Raub, E., Z. Metallkunde, 45 (1954) pp. 23-30, cited in M. Hansen, Constitution of Binary Alloys, McGraw-Hill (1958) p. 870.

Table 1. Time-Temperature Matrix for Conditioning of Specimens.

Temperature °C (K)	Times for specimen conditioning		
1400 (1673)	1 hr	4 hr	16 hr
1300 (1573)	10 hr	40 hr	160 hr
1150 (1423)	100 hr	400 hr	1600 hr
1000 (1273)	1000 hr	4000 hr	12000 hr

Table 2. Diffusion Zone Thickness - Mo>Ir.

Temperature °C (K)	Width of Mo>Ir Diffusion Zone in μm versus Time		
	1 hr	4 hr	16 hr
1400 (1673)	NDZ	NDZ	15.5
	10 hr	40 hr	160 hr
1300 (1573)	NDZ	13.0	20.5
	100 hr	400 hr	1600 hr
1150 (1423)	NDZ	10.0	21.5
	1000 hr	4000 hr	12000 hr
1000 (1273)	2.0	6.5	12.0

* NDZ - No diffusion zone.

Table 3. Diffusion Zone Thickness - Ir>Mo.

Temperature °C (K)	Width of Ir>Mo Diffusion Zone in μm versus Time		
1400 (1673)	1 hr	4 hr	16 hr
	NDZ	NDZ	4.0
1300 (1573)	10 hr	40 hr	160 hr
	NDZ	4.5	8.5
1150 (1423)	100 hr	400 hr	1600 hr
	NDZ	3.5	7.7
1000 (1273)	1000 hr	4000 hr	12000 hr
	NDZ	NDZ	NDZ

* NDZ - No diffusion zone.

Table 4. Diffusion Zone Thickness - Ir>T-111.

Temperature °C (K)	Width of Ir>T-111 Diffusion Zone in μm versus Time		
1400 (1673)	1 hr	4 hr	16 hr
	1.5	2.5	3.7
1300 (1573)	10 hr	40 hr	160 hr
	3.5	2.5	5.0
1150 (1423)	100 hr	400 hr	1600 hr
	NDZ	1.0	3.0
1000 (1273)	1000 hr	4000 hr	12000 hr
	1.0	3.5	5.0

* NDZ - No diffusion zone.

Table 5. Diffusion Zone Thickness - Ta>Ir.

Temperature °C (K)	Width of Ta>Ir Diffusion Zone in μm versus Time		
1400 (1673)	1 hr	4 hr	16 hr
	2.0	2.5	4.5
1300 (1573)	10 hr	40 hr	160 hr
	3.2	5.0	7.0
1150 (1423)	100 hr	400 hr	1600 hr
	3.5	6.5	8.7
1000 (1273)	1000 hr	4000 hr	12000 hr
	NDZ	NDZ	NDZ

* NDZ - No diffusion zone.

Table 6. Diffusivity and Goodness of Fit - Mo>Ir.

	Mo>Ir fit to measurement data		
Temperature °C (K)	Diffusivity (μm^2/hr.)	y intercept	R^2
1400 (1673)	NDZ	NDZ	NDZ
1300 (1573)	1.58E-01	85.25	1.00
1150 (1423)	2.28E-02	-20.75	1.00
1000 (1273)	9.60E-04	-8.69	1.00

* NDZ - No diffusion zone.

Table 7. Diffusivity and Goodness of Fit - Ir>Mo.

	Ir>Mo fit to measurement data		
Temperature °C (K)	Diffusivity (μm^2/hr.)	y intercept	R^2
1400 (1673)	NDZ	NDZ	NDZ
1300 (1573)	3.27E-02	2.92	1.00
1150 (1423)	3.01E-03	-3.69	1.00
1000 (1273)	NDZ	NDZ	NDZ

* NDZ - No diffusion zone.

Table 8. Diffusivity and Goodness of Fit - Ir>T-111.

	Ir>T-111 fit to measurement data		
Temperature °C (K)	Diffusivity (μm^2/hr.)	y intercept	R^2
1400 (1673)	5.65E-02	2.28	0.98
1300 (1573)	7.95E-03	7.13	0.76
1150 (1423)	0.604	-7.00	1.00
1000 (1273)	0.906	-11.25	0.99

Table 9. Diffusivity and Goodness of Fit - Ta>Ir.

	Ta>Ir fit to measurement data		
Temperature °C (K)	Diffusivity (μm^2/hr.)	y intercept	R^2
1400 (1673)	8.36E-02	2.42	0.99
1300 (1573)	1.81E-02	11.37	0.96
1150 (1423)	2.43	-20.62	0.99
1000 (1273)	NDZ	NDZ	NDZ

* NDZ - No diffusion zone.

Table 10. Parameters for Bidirectional Diffusion.

	Fit to diffusion coefficients		
Diffusion direction	D_o (μm^2/hr.)	Activation Energy (cal/mole)	R^2
Ta>Ir	1.32E+11	72,800	0.61
Ir>T-111	1.47E+07	42,000	0.63
Mo>Ir	5.05E+08	67,800	0.99
Ir>Mo	2.23E+08	70,500	1.00

Table 11. Comparison of Predicted and Observed Diffusion Zone Thickness - Mo>Ir.

Temperature °C (K)		Width of Mo>Ir Diffusion Zone in μm		
		1 hr	4 hr	16 hr
1400 (1673)	Predicted	2.95	5.91	11.81
	Observed	0.0	0.0	15.5
	Difference	2.95	5.91	-3.69
		10 hr	40 hr	160 hr
1300 (1573)	Predicted	4.87	9.74	19.48
	Observed	0.0	13.0	20.5
	Difference	4.87	-3.26	-1.02
		100 hr	400 hr	1600 hr
1150 (1423)	Predicted	4.88	9.77	19.53
	Observed	0.0	10.0	21.5
	Difference	4.88	-0.23	-1.97
		1000 hr	4000 hr	12000 hr
1000 (1273)	Predicted	3.64	7.28	12.61
	Observed	2.0	6.5	12.0
	Difference	1.64	0.78	0.61

Table 12. Comparison of Predicted and Observed Diffusion Zone Thickness - Ir>Mo.

Temperature °C (K)		Width of Ir>Mo Diffusion Zone in μm		
		1 hr	4 hr	16 hr
1400 (1673)	Predicted	1.29	2.58	5.17
	Observed	0.0	0.0	4.0
	Difference	1.29	2.58	1.17
		10 hr	40 hr	160 hr
1300 (1573)	Predicted	2.09	4.18	8.36
	Observed	0.0	4.5	8.5
	Difference	2.09	-0.32	-0.14
		100 hr	400 hr	1600 hr
1150 (1423)	Predicted	1.99	3.99	7.97
	Observed	0.0	3.5	7.8
	Difference	1.99	0.49	0.22
		1000 hr	4000 hr	12000 hr
1000 (1273)	Predicted	1.50	2.99	5.18
	Observed	0.0	0.0	0.0
	Difference	1.50	2.99	5.18

Table 13. Comparison of Predicted and Observed Diffusion Zone Thickness - Ir>T-111.

Temperature °C (K)		Width of Ir>T-111 Diffusion Zone in μm		
		1 hr	4 hr	16 hr
1400 (1673)	Predicted	24.72	49.43	98.86
	Observed	0.0	0.0	4.0
	Difference	24.72	49.43	94.86
		10 hr	40 hr	160 hr
1300 (1573)	Predicted	52.24	104.49	208.97
	Observed	0.0	4.5	8.5
	Difference	52.24	99.99	200.47
		100 hr	400 hr	1600 hr
1150 (1423)	Predicted	81.19	162.38	324.76
	Observed	0.0	3.5	7.8
	Difference	81.19	158.88	317.01
		1000 hr	4000 hr	12000 hr
1000 (1273)	Predicted	106.75	213.49	369.78
	Observed	0.0	0.0	0.0
	Difference	106.75	213.49	369.78

Table 14. Comparison of Predicted and Observed Diffusion Zone Thickness - Ta>Ir.

Temperature °C (K)		Width of Ta>Ir Diffusion Zone in μm		
		1 hr	4 hr	16 hr
1400 (1673)	Predicted	22.25	44.49	88.99
	Observed	2.0	2.5	4.5
	Difference	20.25	41.99	84.49
		10 hr	40 hr	160 hr
1300 (1573)	Predicted	34.98	69.95	139.90
	Observed	3.3	5.0	7.0
	Difference	31.73	64.95	132.90
		100 hr	400 hr	1600 hr
1150 (1423)	Predicted	32.25	64.50	129.00
	Observed	3.5	6.5	8.8
	Difference	28.75	58.00	120.25
		1000 hr	4000 hr	12000 hr
1000 (1273)	Predicted	22.14	44.28	76.70
	Observed	0.0	0.0	0.0
	Difference	22.14	44.28	76.70

Table 15. Combined Diffusion Zone Thickness - Mo/Ir.

Temperature °C (K)	Width of Mo+Ir Diffusion Zone in μm versus Time		
1400 (1673)	1 hr	4 hr	16 hr
	NDZ	NDZ	19.5
1300 (1573)	10 hr	40 hr	160 hr
	NDZ	17.5	29.0
1150 (1423)	100 hr	400 hr	1600 hr
	NDZ	13.5	29.3
1000 (1273)	1000 hr	4000 hr	12000 hr
	2.0	6.5	12.0

* NDZ - No diffusion zone.

Table 16. Combined Diffusion Zone Thickness - Ir/T-111.

Temperature °C (K)	Width of Ta+Ir Diffusion Zone in μm versus Time		
1400 (1673)	1 hr	4 hr	16 hr
	3.5	5.0	8.3
1300 (1573)	10 hr	40 hr	160 hr
	6.8	7.5	12.0
1150 (1423)	100 hr	400 hr	1600 hr
	3.5	7.5	11.8
1000 (1273)	1000 hr	4000 hr	12000 hr
	1.0	3.5	5.0

Table 17. Diffusivity and Goodness of Fit for Combined Diffusion Zone Thickness - Mo/Ir.

	Total (Mo+Ir) fit to measurement data		
Temperature °C (K)	Diffusivity (μm^2/hr.)	y intercept	R^2
1400 (1673)	NDZ	NDZ	NDZ
1300 (1573)	3.36E-01	128.00	1.00
1150 (1423)	4.23E-02	-42.18	1.00
1000 (1273)	9.60E-04	-8.69	1.00

* NDZ - No diffusion zone.

Table 18. Diffusivity and Goodness of Fit for Combined Diffusion Zone Thickness - Ir/T-111.

	Total (Ta+Ir) fit to measurement data		
Temperature °C (K)	Diffusivity (μm^2/hr.)	y intercept	R^2
1400 (1673)	2.78E-01	9.32	0.99
1300 (1573)	5.11E-02	34.50	0.99
1150 (1423)	5.99E-03	13.28	0.97
1000 (1273)	1.56E-04	1.07	0.95

Table 19. Parameters for Lumped Diffusion Zones.

	Fit to diffusion coefficients		
Diffusion direction	D_o (μm^2/hr.)	Activation Energy (cal/mole)	R^2
Ta+Ir	3.84E+09	77,400	0.99
Mo+Ir	3.03E+10	77,900	0.99

Table 20. Comparison of Predicted and Observed Combined Diffusion Zone Thickness - Mo/Ir.

Temperature °C (K)		Width of Mo+Ir Diffusion Zone in μm		
		1 hr	4 hr	16 hr
1400 (1673)	Predicted	4.93	9.86	19.72
	Observed	0.0	0.0	19.5
	Difference	4.93	9.86	0.22
		10 hr	40 hr	160 hr
1300 (1573)	Predicted	7.38	14.76	29.52
	Observed	0.0	17.5	29.0
	Difference	7.38	-2.74	0.52
		100 hr	400 hr	1600 hr
1150 (1423)	Predicted	6.20	12.40	24.79
	Observed	0.0	13.5	29.3
	Difference	6.20	-1.10	-4.46
		1000 hr	4000 hr	12000 hr
1000 (1273)	Predicted	3.64	7.28	12.61
	Observed	2.0	6.5	12.0
	Difference	1.64	0.78	0.61

Table 21. Comparison of Predicted and Observed Combined Diffusion Zone Thickness - Ir/T-111.

Temperature °C (K)		Width of Ta+Ir Diffusion Zone in μm		
		1 hr	4 hr	16 hr
1400 (1673)	Predicted	1.90	3.80	7.59
	Observed	3.5	5.0	8.3
	Difference	-1.60	-1.20	-0.66
		10 hr	40 hr	160 hr
1300 (1573)	Predicted	2.87	5.73	11.46
	Observed	6.8	7.5	12.0
	Difference	-3.88	-1.77	-0.54
		100 hr	400 hr	1600 hr
1150 (1423)	Predicted	2.30	4.60	9.21
	Observed	3.5	7.5	11.8
	Difference	-1.20	-2.90	-2.54
		1000 hr	4000 hr	12000 hr
1000 (1273)	Predicted	1.53	3.05	5.29
	Observed	1.0	3.5	5.0
	Difference	0.53	-0.45	0.29

Table 22. Predicted diffusion zone thickness - Mo>Ta.

Temperature °C (K)	Predicted Width of Mo>Ta Diffusion Zone in μm versus Time		
1400 (1673)	1 hr	4 hr	16 hr
	0.05	0.09	0.18
1300 (1573)	10 hr	40 hr	160 hr
	0.07	0.13	0.26
1150 (1423)	100 hr	400 hr	1600 hr
	0.05	0.11	0.21
1000 (1273)	1000 hr	4000 hr	12000 hr
	0.03	0.06	0.11

Table 23. Predicted diffusion zone thickness - Ta>Mo.

Temperature °C (K)	Predicted Width of Ta>Mo Diffusion Zone in μm versus Time		
1400 (1673)	1 hr	4 hr	16 hr
	0.02	0.03	0.06
1300 (1573)	10 hr	40 hr	160 hr
	0.02	0.04	0.08
1150 (1423)	100 hr	400 hr	1600 hr
	0.02	0.03	0.07
1000 (1273)	1000 hr	4000 hr	12000 hr
	0.01	0.02	0.03

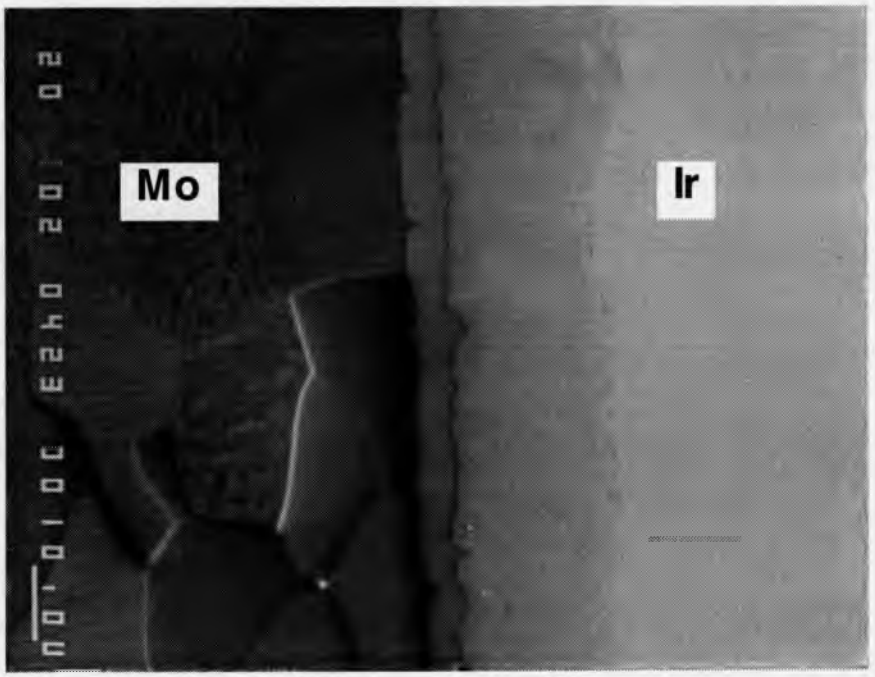

Figure 1. Secondary electron image of molybdenum-iridium diffusion couple, 1150 degrees Celsius - 1600 hours, 1000 x.

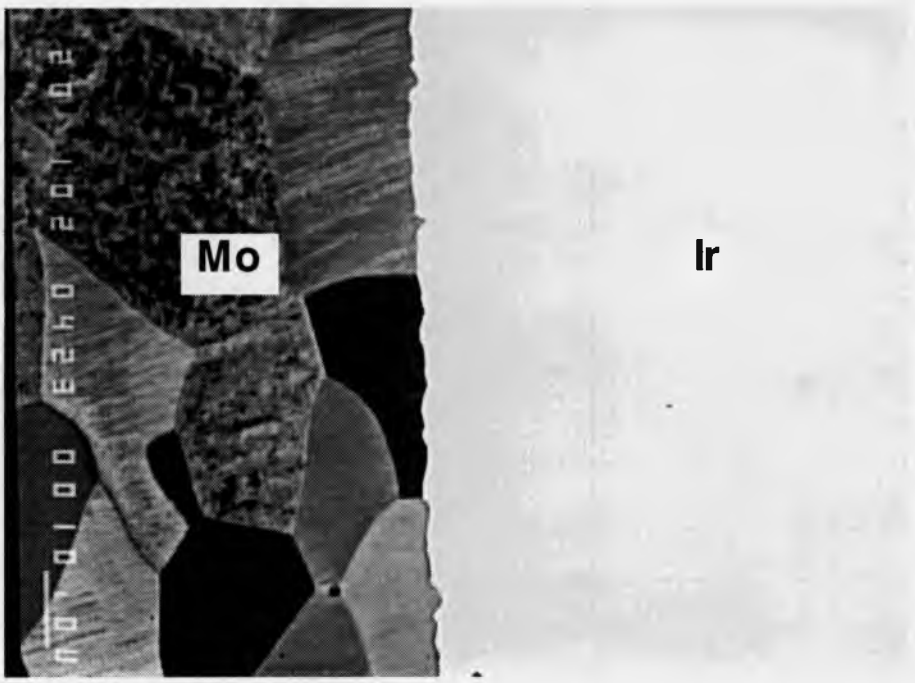

Figure 2. Backscattered electron image of molybdenum - iridium diffusion couple showing molybdenum, , 1150 degrees Celsius - 1600 hours, 1000 x.

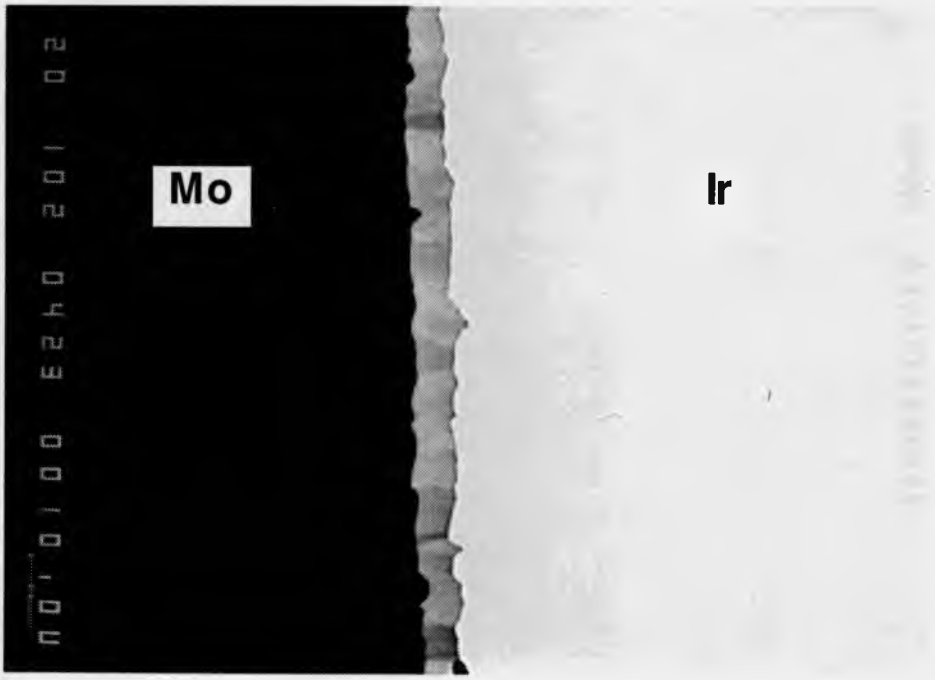

Figure 3. Backscattered electron image of molybdenum - irridium diffusion couple showing a molybdenum rich diffusion zone, 1150 degrees Celsius - 1600 hours, 1000 x.

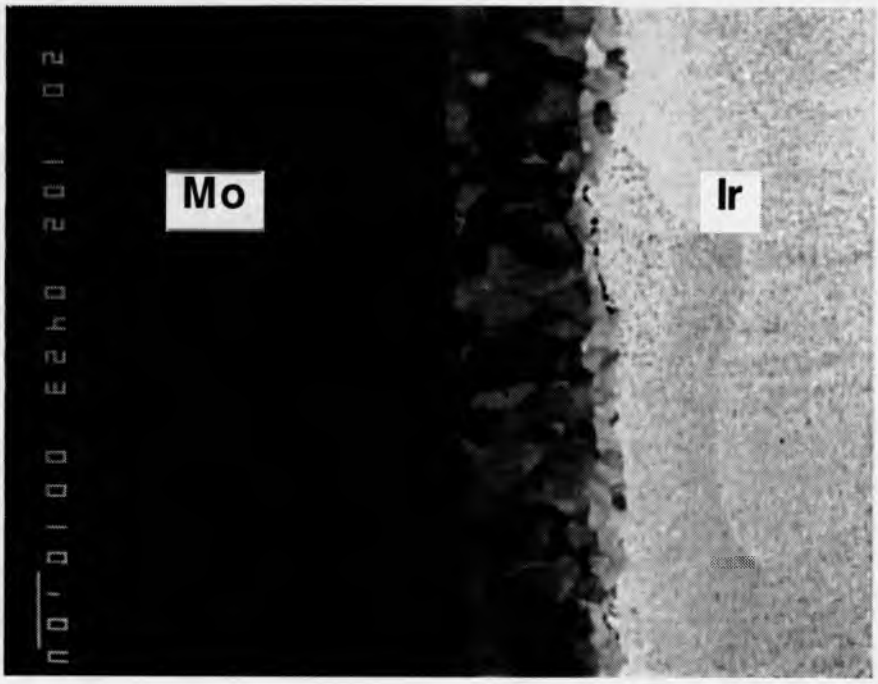

Figure 4. Backscattered electron image of molybdenum - iridium diffusion couple showing iridium and iridium rich diffusion zone, 1150 degrees Celsius - 1600 hours, 1000 x.

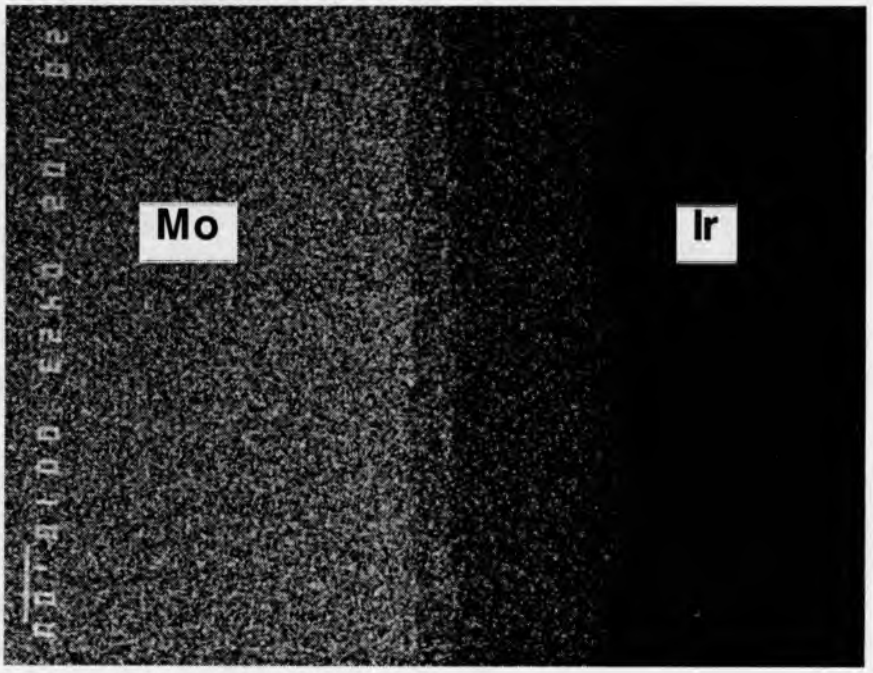

Figure 5. Molybdenum x-ray dot map of molybdenum - iridium diffusion couple, 1150 degrees Celsius - 1600 hours, 1000 x.

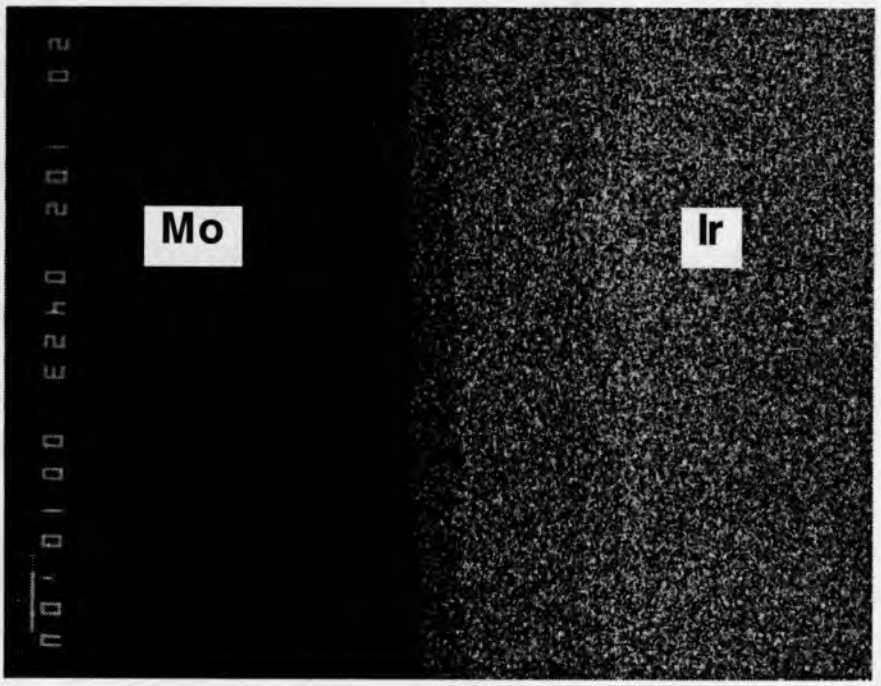

Figure 6. Iridium x-ray dot map of molybdenum - iridium diffusion couple, 1150 degrees Celsius - 1600 hours, 1000 x.

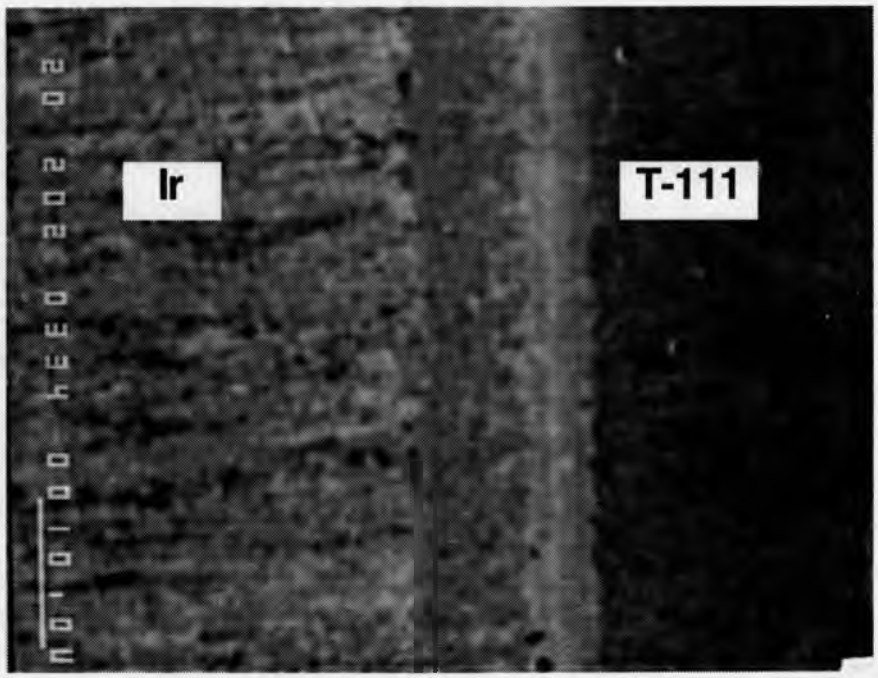

Figure 7. Secondary electron image of iridium - T-111 diffusion couple, 1300 degrees Celsius - 160 hours, 2000 x.

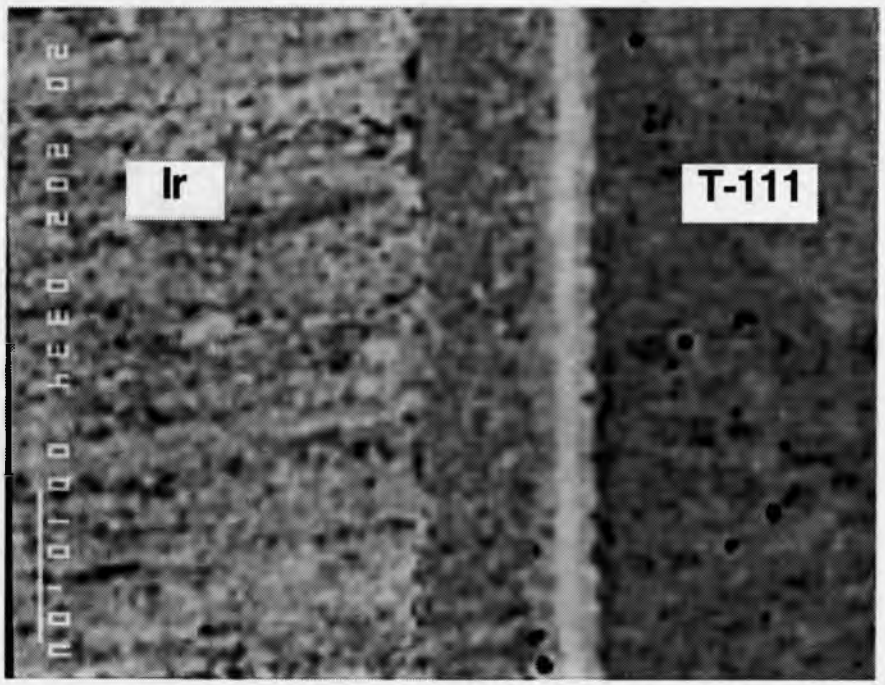

Figure 8. Backscattered electron image of iridium - T-111 diffusion couple, 1300 degrees Celsius - 160 hours, 2000x.

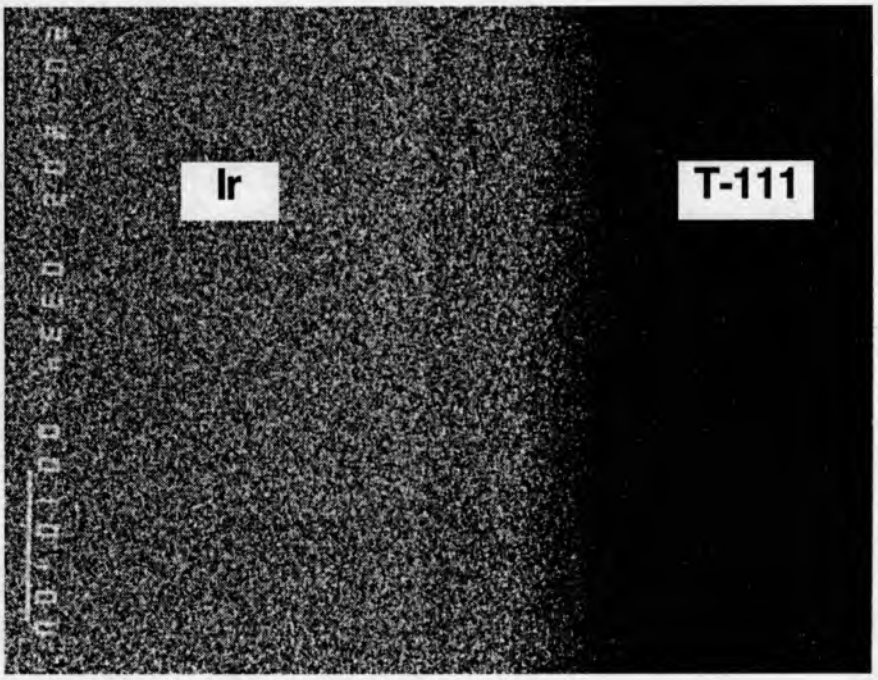

Figure 9. Iridium x-ray dot map of iridium - T-111 diffusion couple, 1300 degrees Celsius - 160 hours, 2000 x.

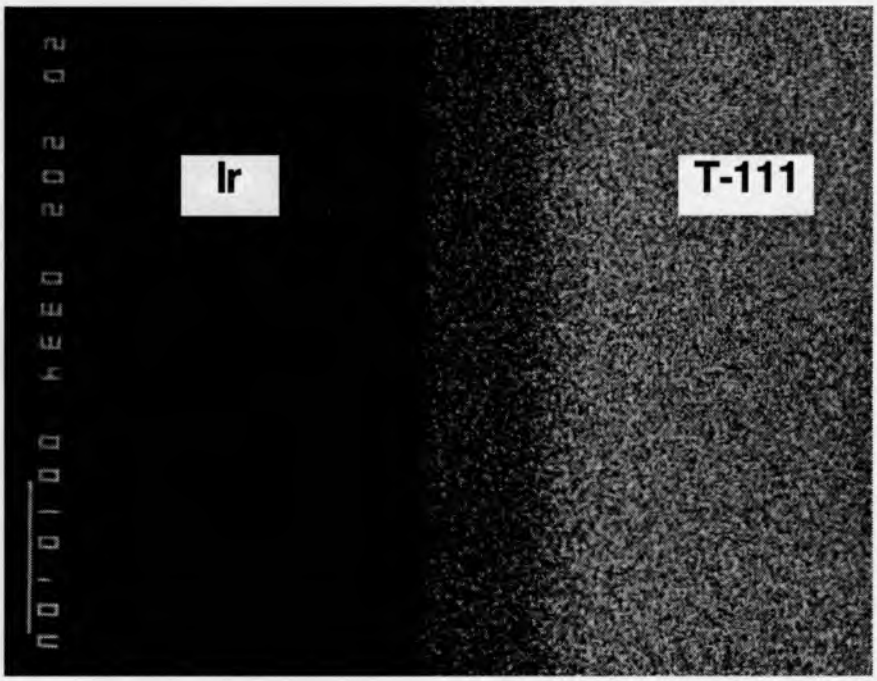

Figure 10. Tantalum x-ray dot map of iridium - T-111 diffusion couple, 1300 degrees Celsius - 160 hours, 2000 x.

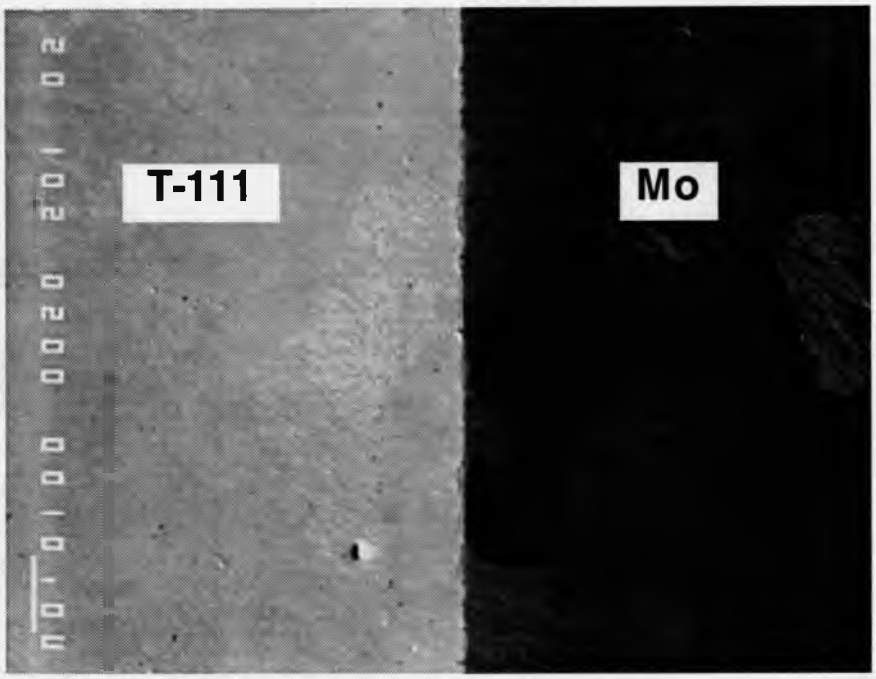

Figure 11. Secondary electron image of molybdenum - T-111 diffusion couple, 1150 degrees Celsius - 400 hours, 1000 x.

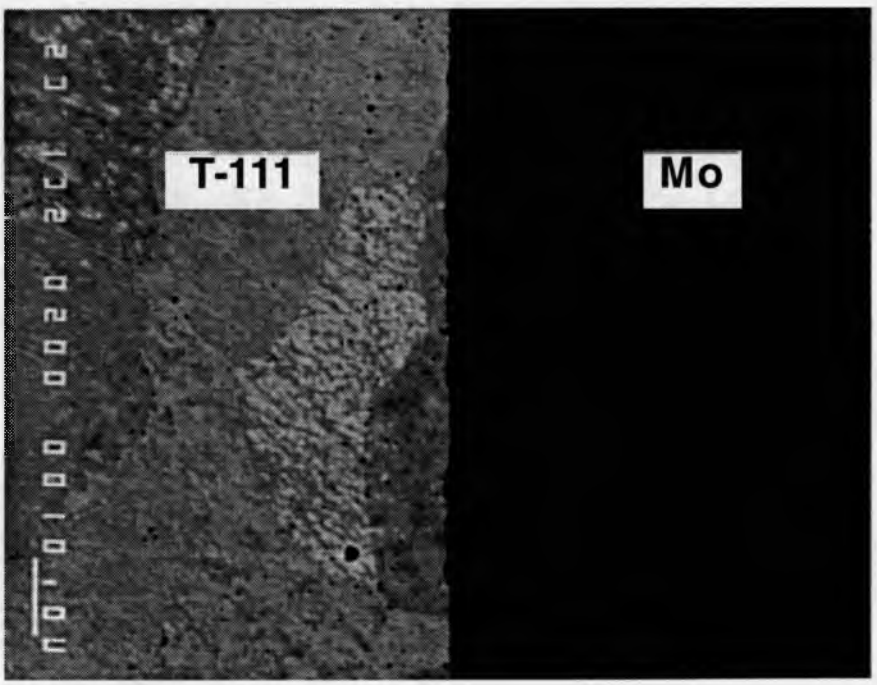

Figure 12. Backscattered electron image of molybdenum - T-111 diffusion couple showing T-111, 1150 degrees Celsius - 400 hours, 1000 x.

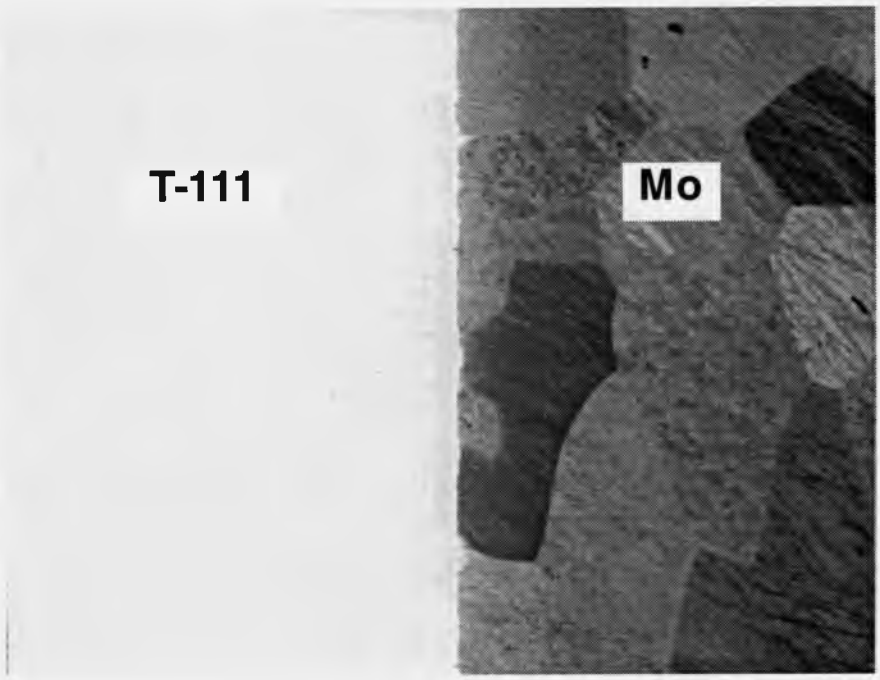

Figure 13. Backscattered electron image of molybdenum - T-111 diffusion couple showing molybdenum, 1150 degrees Celsius - 400 hours, 1000 x.

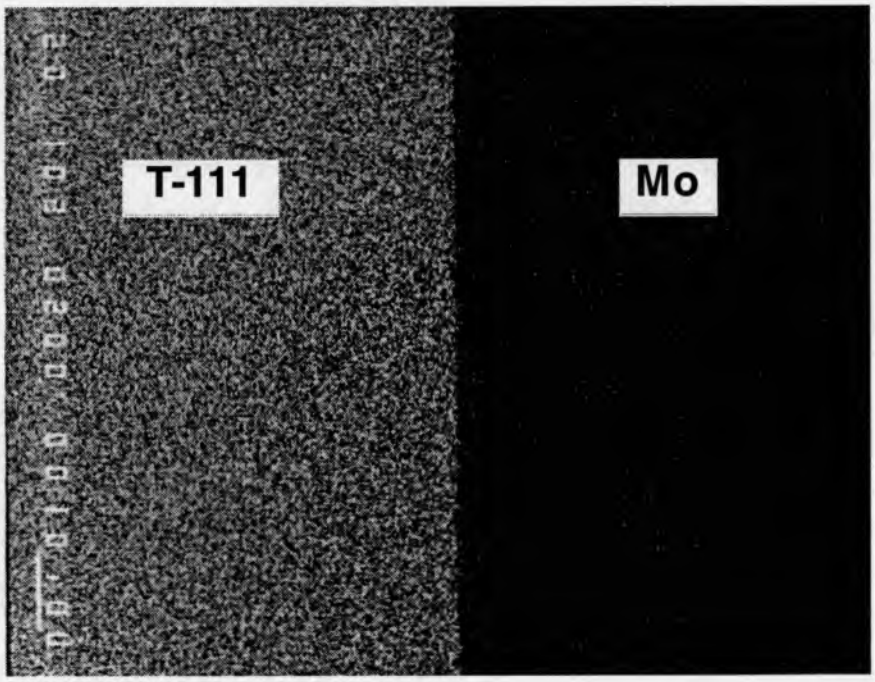

Figure 14. Tantalum x-ray dot map of molybdenum - T-111 diffusion couple, 1150 degrees Celsius - 400 hours, 1000 x.

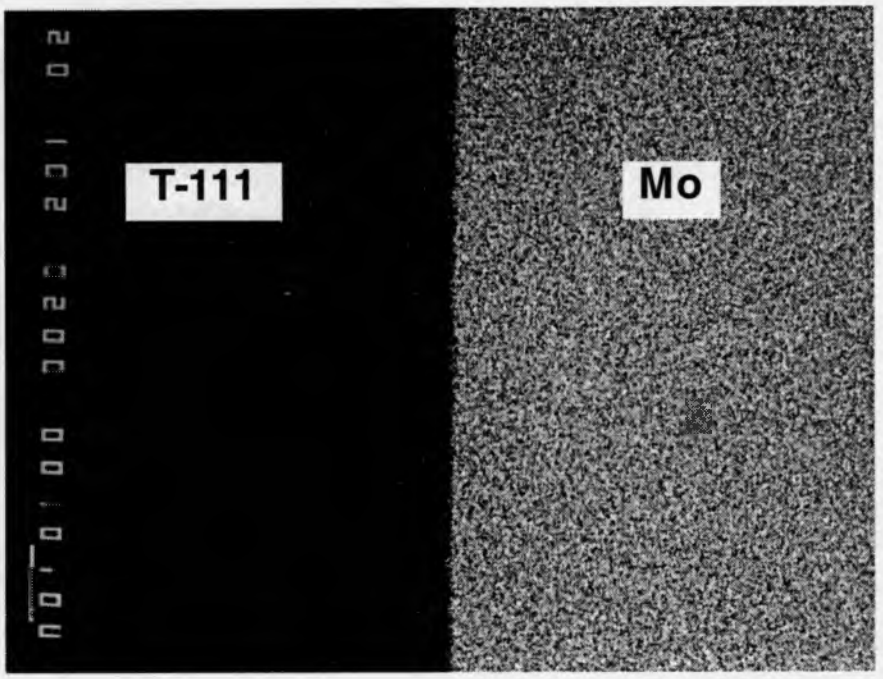

Figure 15. Molybdenum x-ray dot map of molybdenum - T-111 diffusion couple, 1150 degrees Celsius - 400 hours, 1000 x.

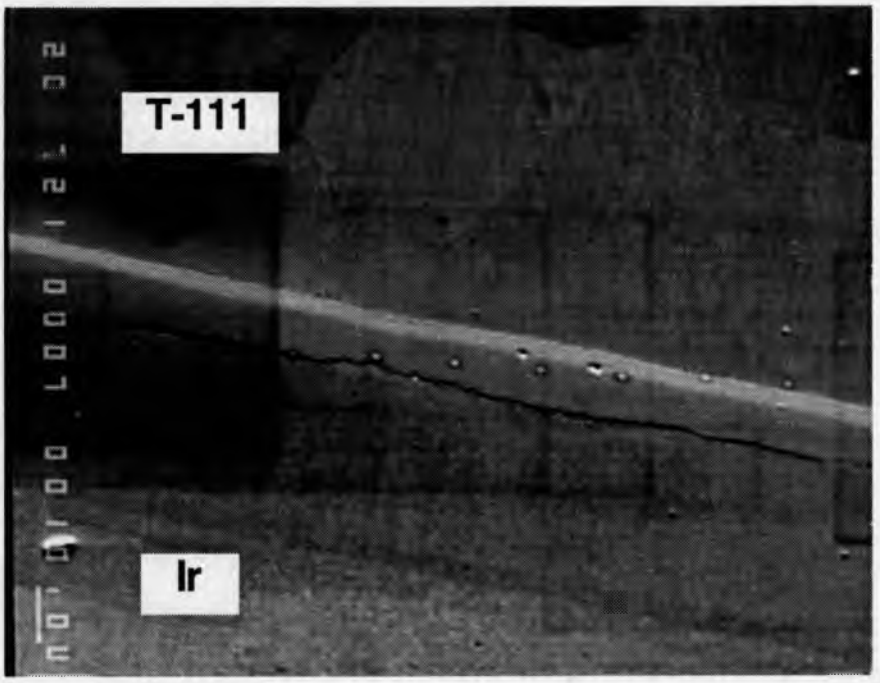

Figure 16. Secondary electron micrograph of region on iridium - T-111 diffusion couple in which linescan was performed, 1150 degrees Celsius - 1600 hours, 720 x.

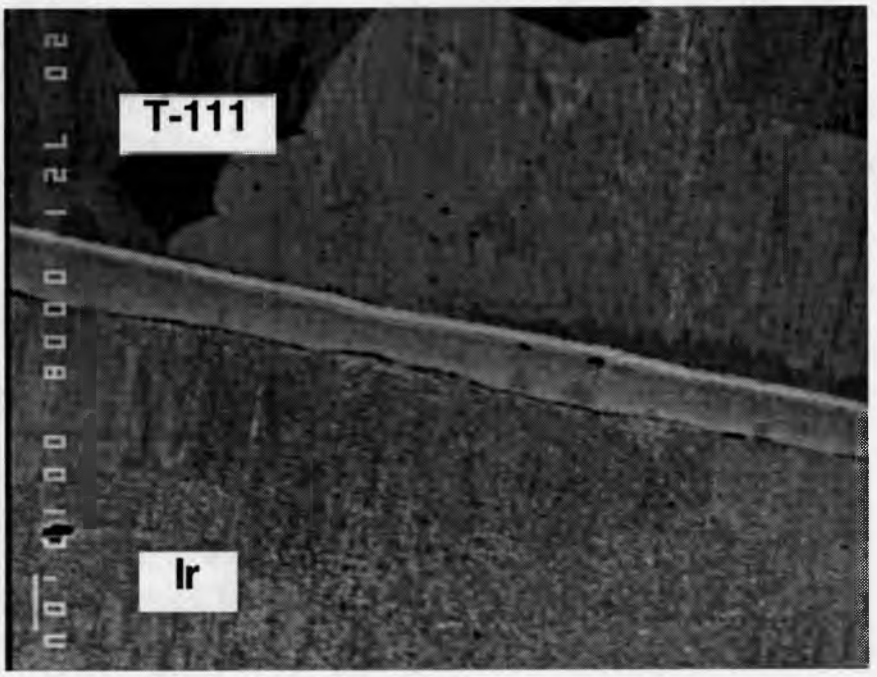

Figure 17. Backscattered electron micrograph of region on iridium - T-111 diffusion couple in which linescan was performed, 1150 degrees Celsius - 1600 hours, 720 x.

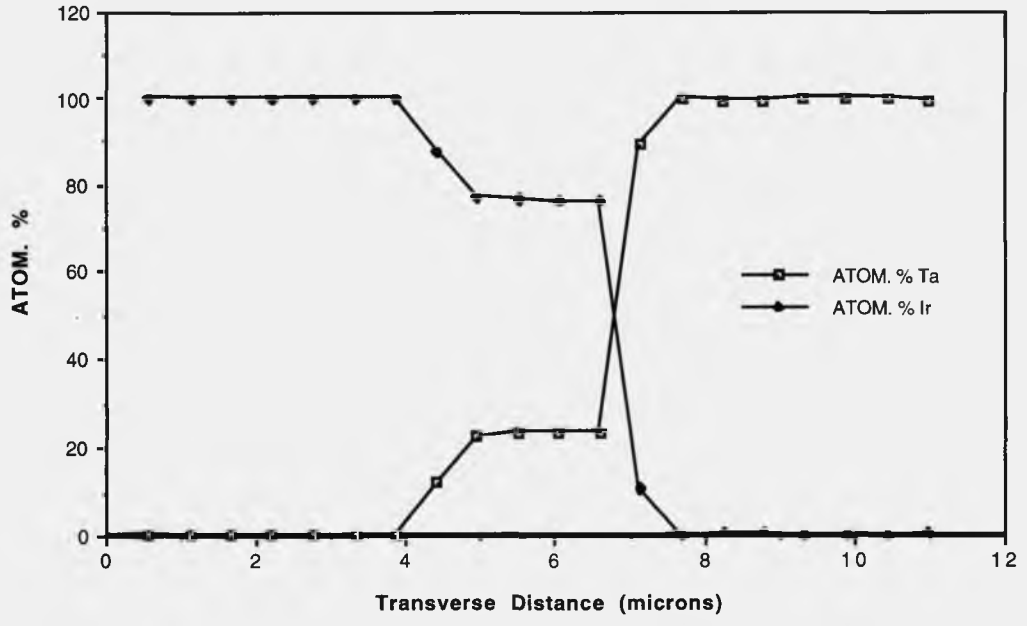

Figure 18. Linescan compositional profile of iridium - T-111 diffusion couple.

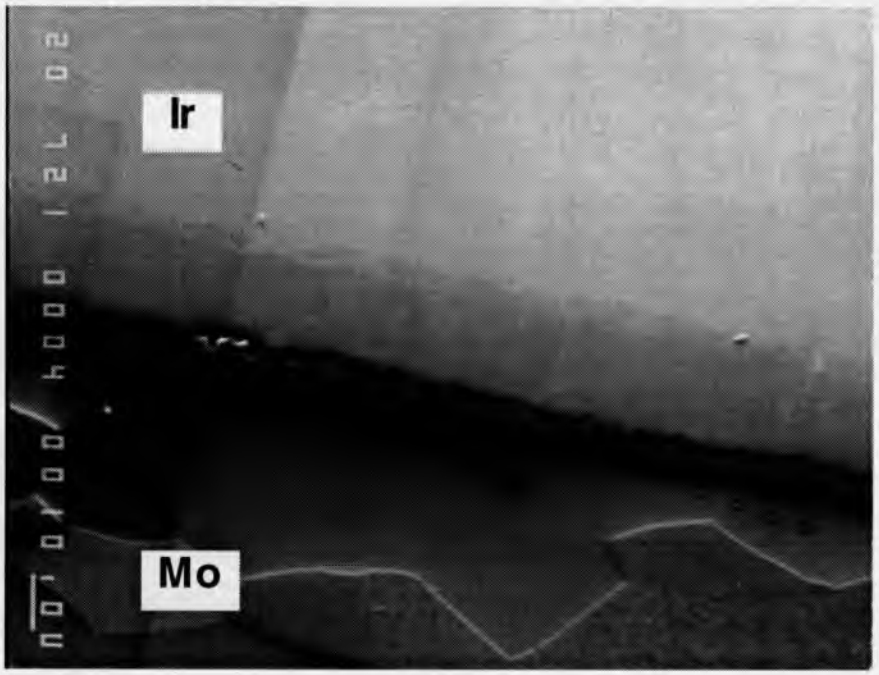

Figure 19. Secondary electron micrograph of region on iridium - molybdenum diffusion couple in which linescan was performed, 1150 degrees Celsius - 1600 hours, 720 x.

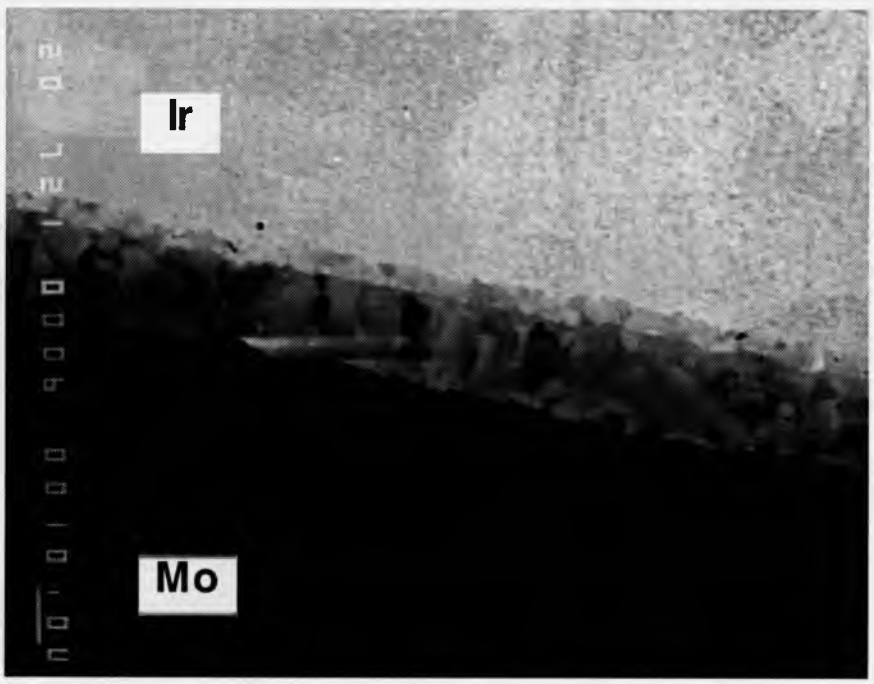

Figure 20. Backscattered electron micrograph of region on iridium - molybdenum diffusion couple in which linescan was performed, 1150 degrees Celsius - 1600 hours, 720 x.

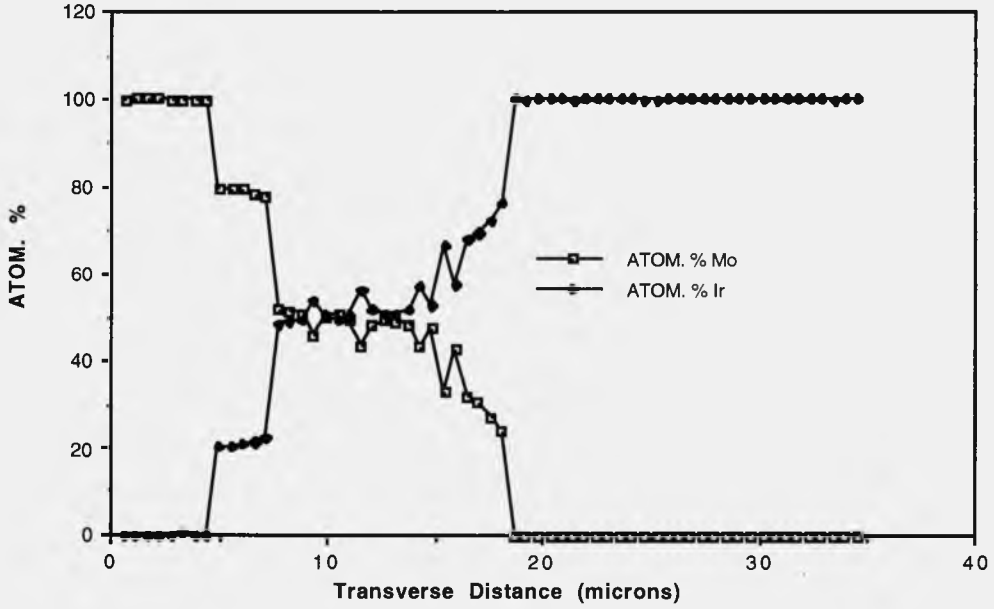

Figure 21. Linescan compositional profile of iridium - molybdenum diffusion couple.

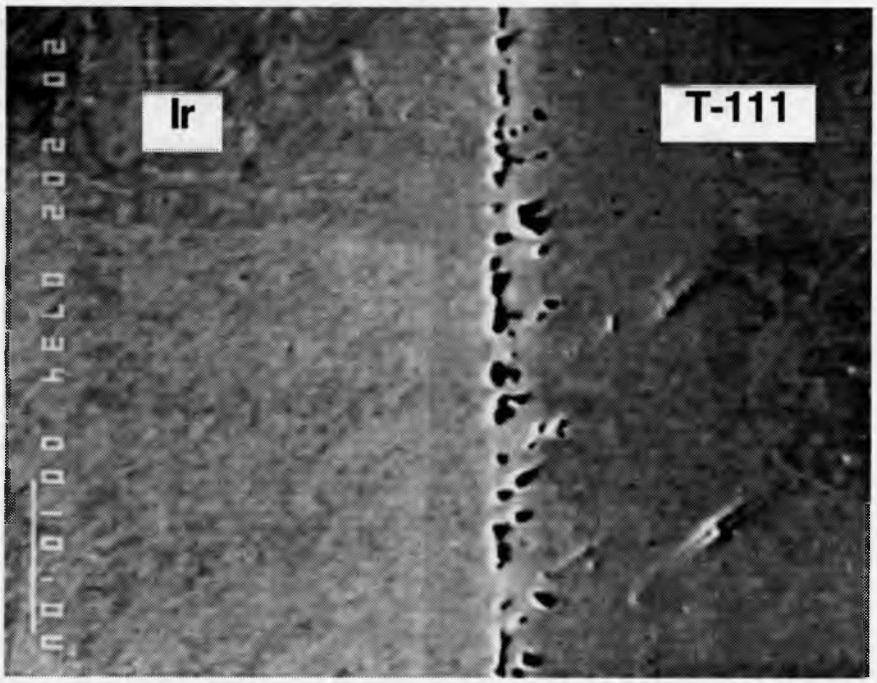

Figure 22. Secondary electron image of voids found in iridium - T-111 diffusion zone, 1300 degrees Celsius - 40 hours, 2000 x.

Appendix I

Diffusion Zone Thickness and Arrhenius Plots

Table A1. Cross Reference Between Tables and Figures.

Figure	Table
A1	2
A2	2
A3	2
A4	3
A5	3
A6	4
A7	4
A8	4
A9	4
A10	5
A11	5
A12	5
A13	6, 10
A14	7, 10
A15	8, 10
A16	9, 10
A17	15
A18	15
A19	15
A20	16
A21	16
A22	16
A23	16
A24	17, 19
A25	18, 19

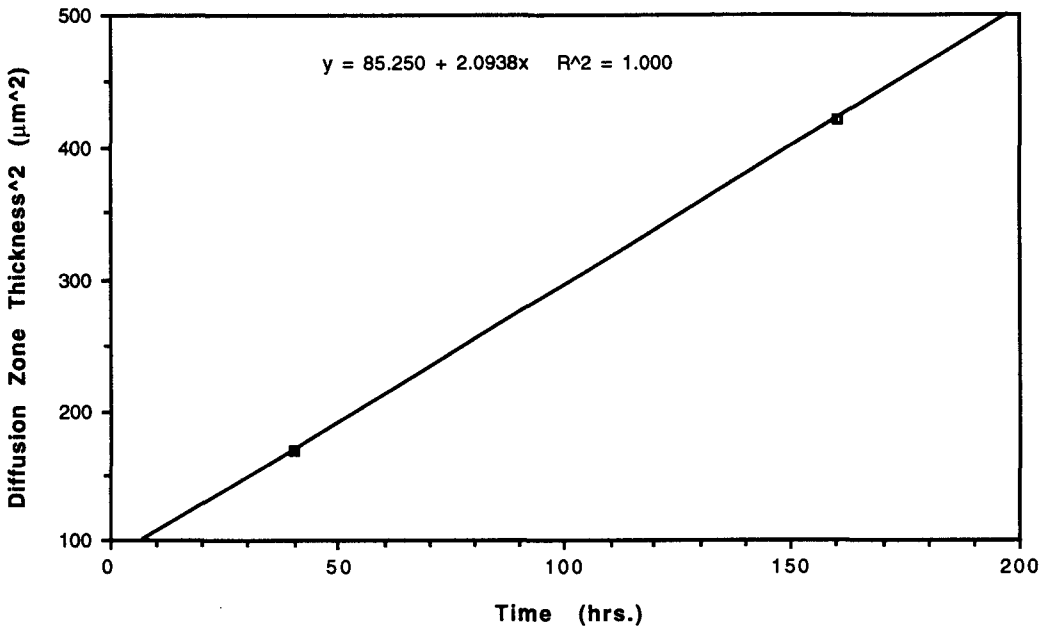

Figure A1. Diffusion Zone Thickness squared versus Time, Mo>Ir, 1300°C.

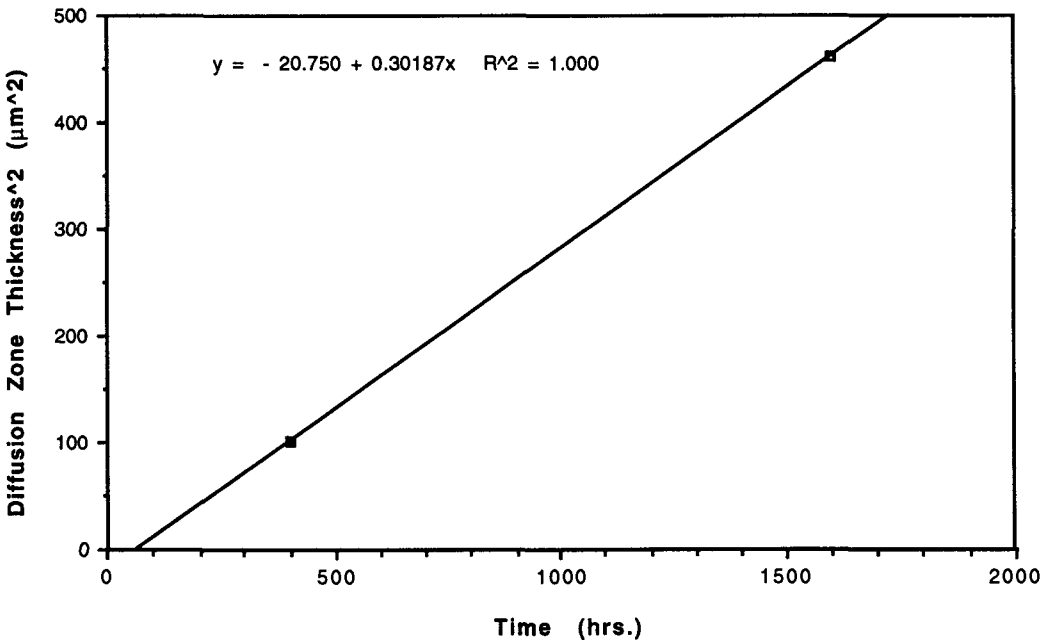

Figure A2. Diffusion Zone Thickness squared versus Time, Mo>Ir, 1150°C.

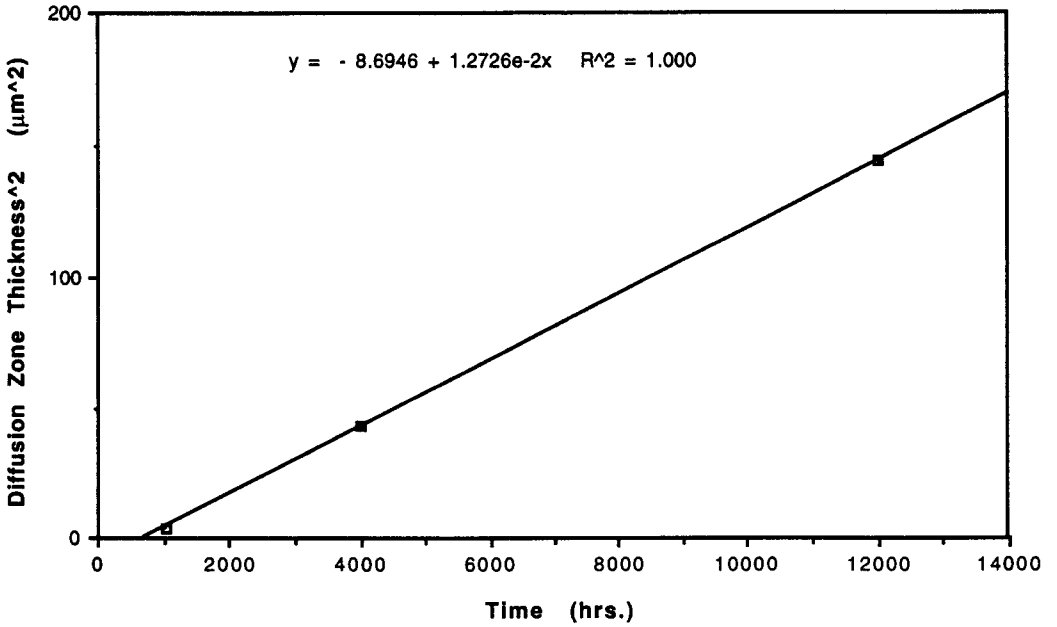

Figure A3. Diffusion Zone Thickness squared versus Time, Mo>Ir, 1000°C.

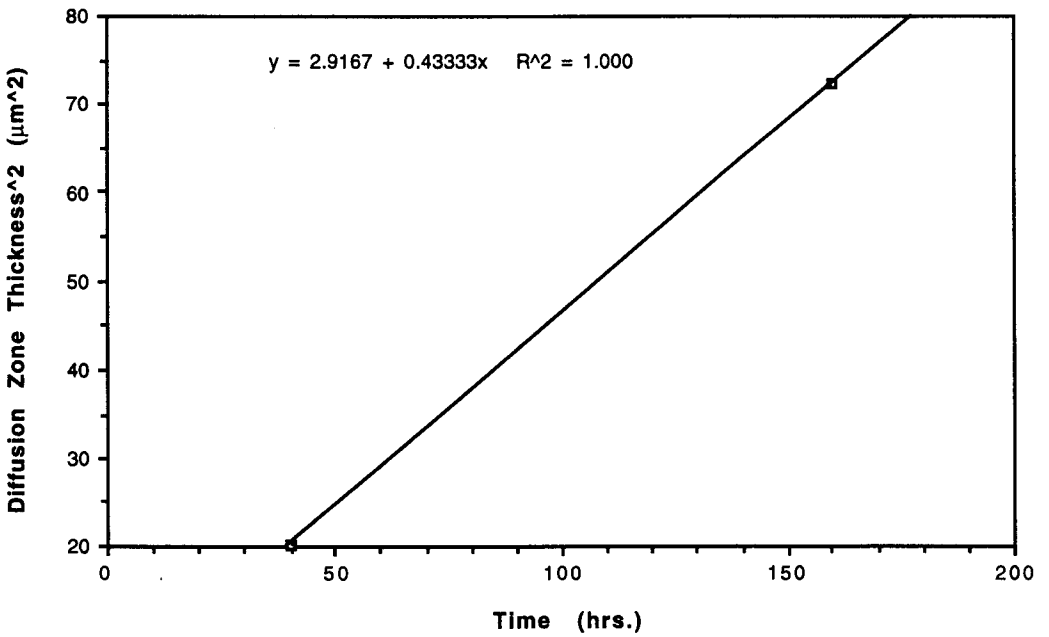

Figure A4. Diffusion Zone Thickness squared versus Time, Ir>Mo, 1300°C.

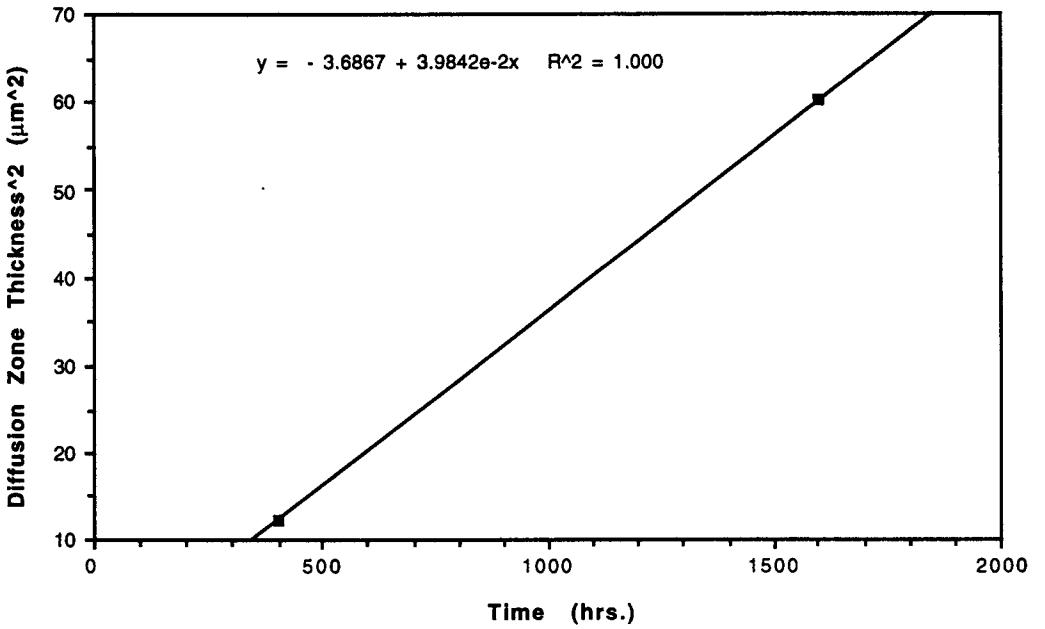

Figure A5. Diffusion Zone Thickness squared versus Time, Ir>Mo, 1150°C.

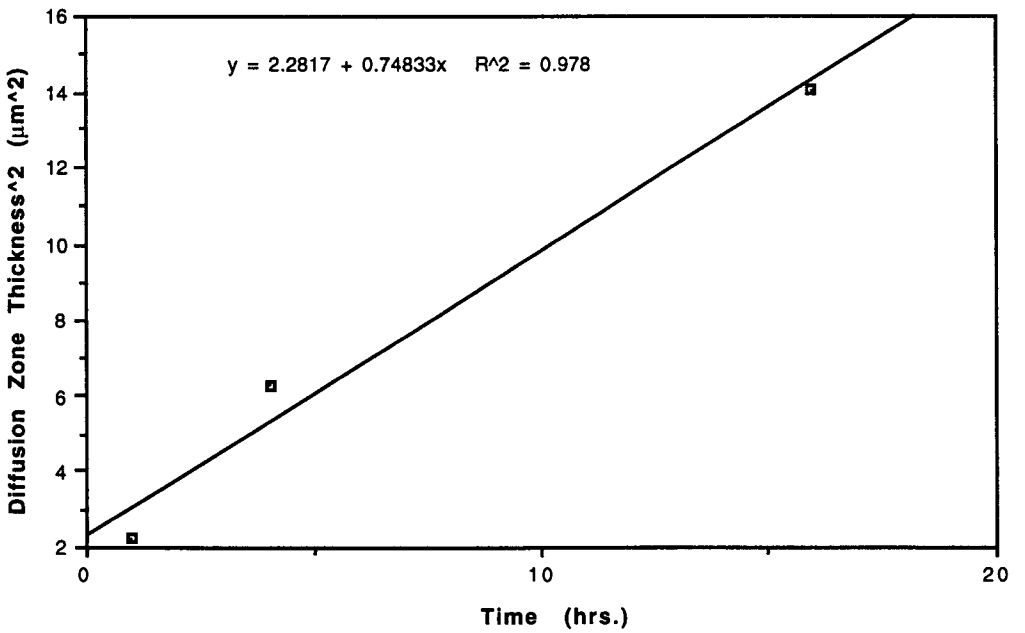

Figure A6. Diffusion Zone Thickness squared versus Time, Ir>T-111, 1400°C.

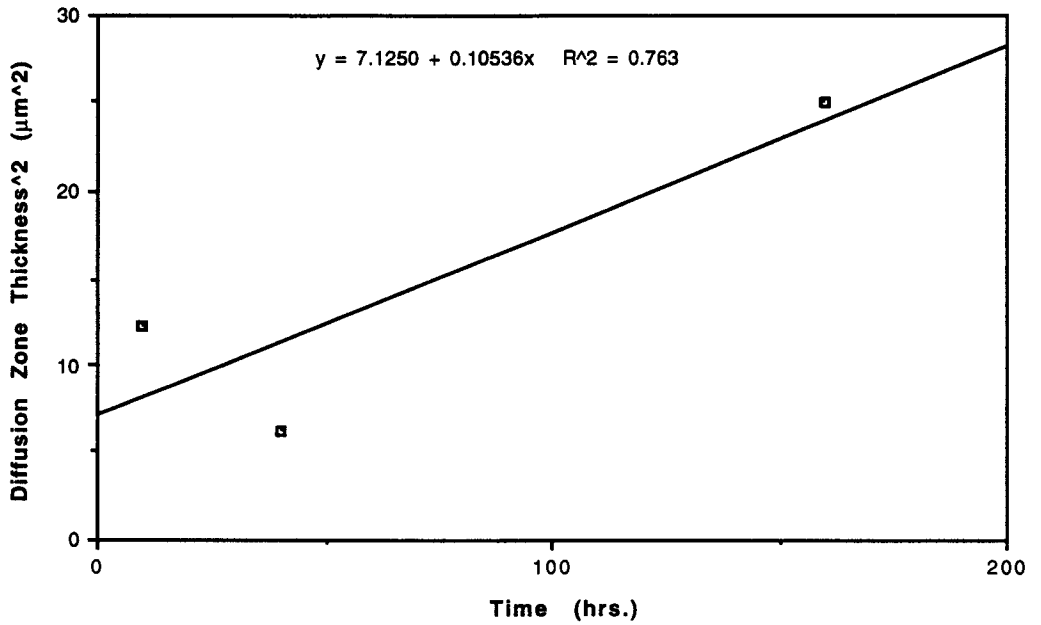

Figure A7. Diffusion Zone Thickness squared versus Time, Ir>T-111, 1300°C.

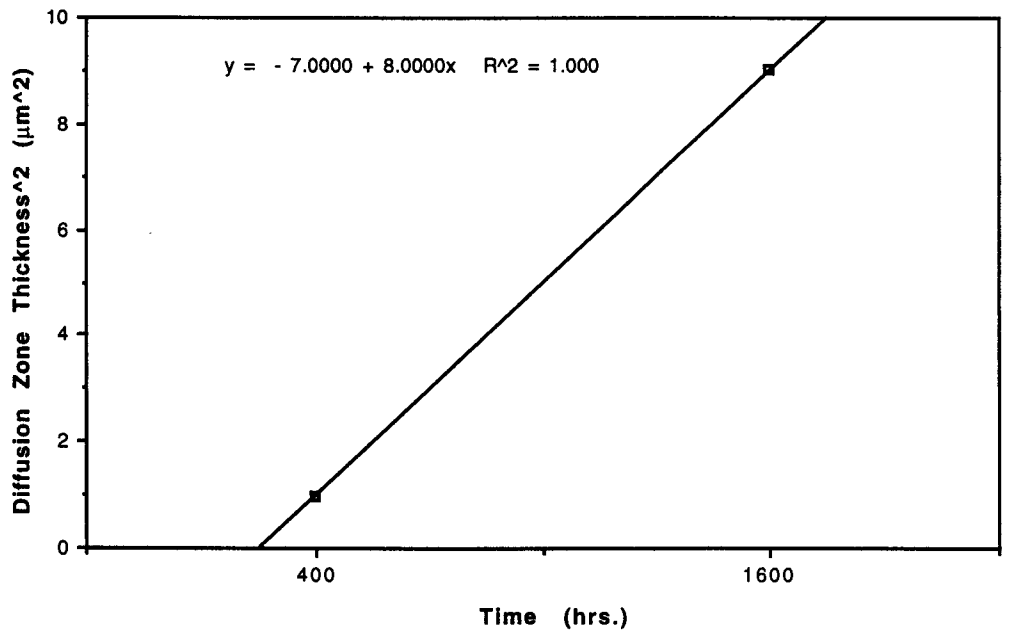

Figure A8. Diffusion Zone Thickness squared versus Time, Ir>T-111, 1150°C.

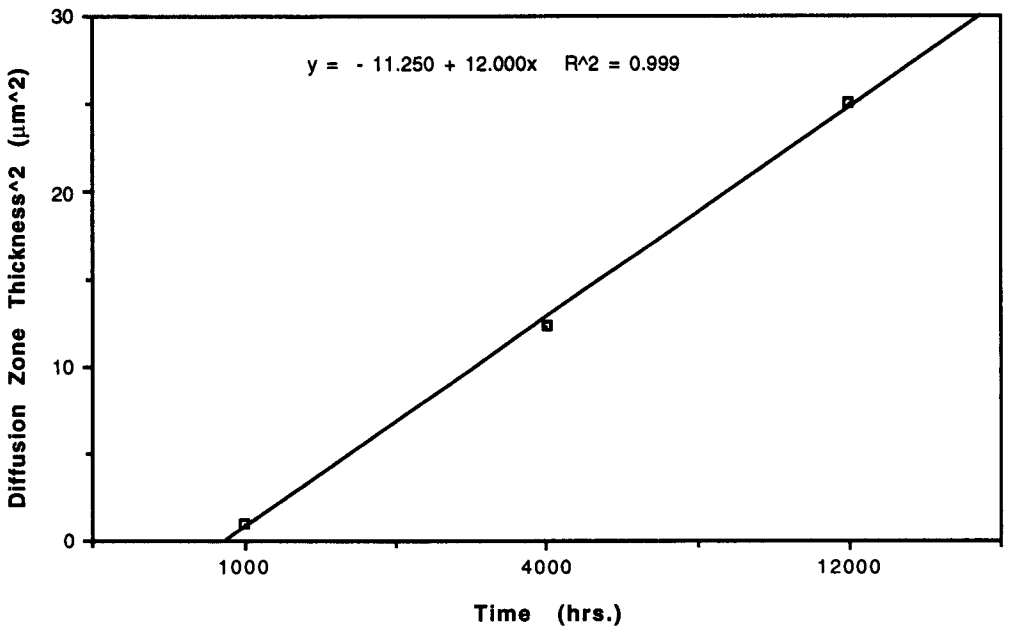

Figure A9. Diffusion Zone Thickness squared versus Time, Ir>T-111, 1000°C.

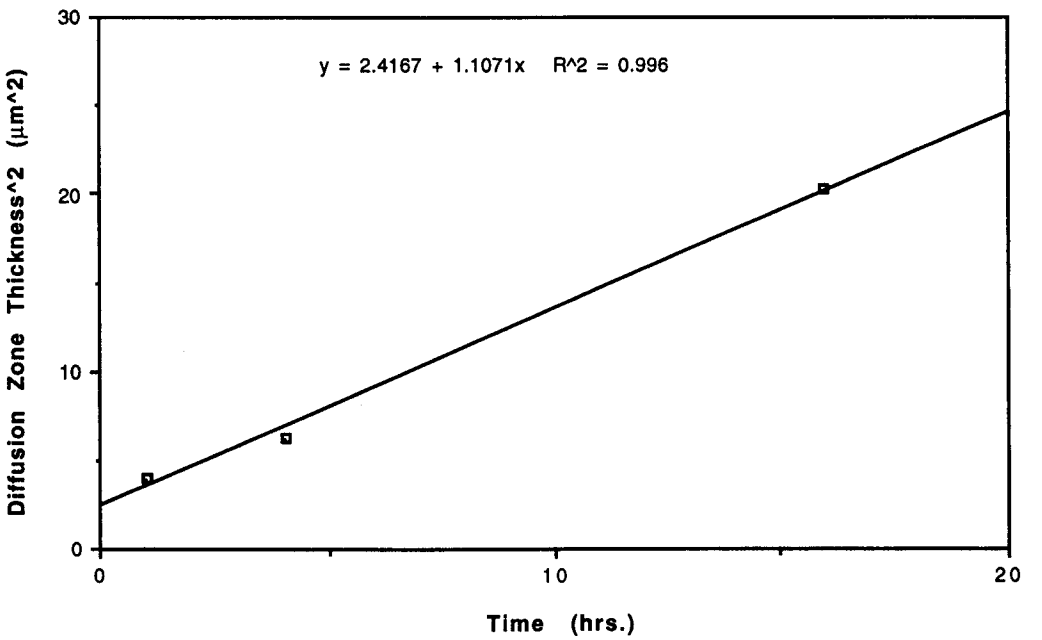

Figure A10. Diffusion Zone Thickness squared versus Time, Ta>Ir, 1400°C.

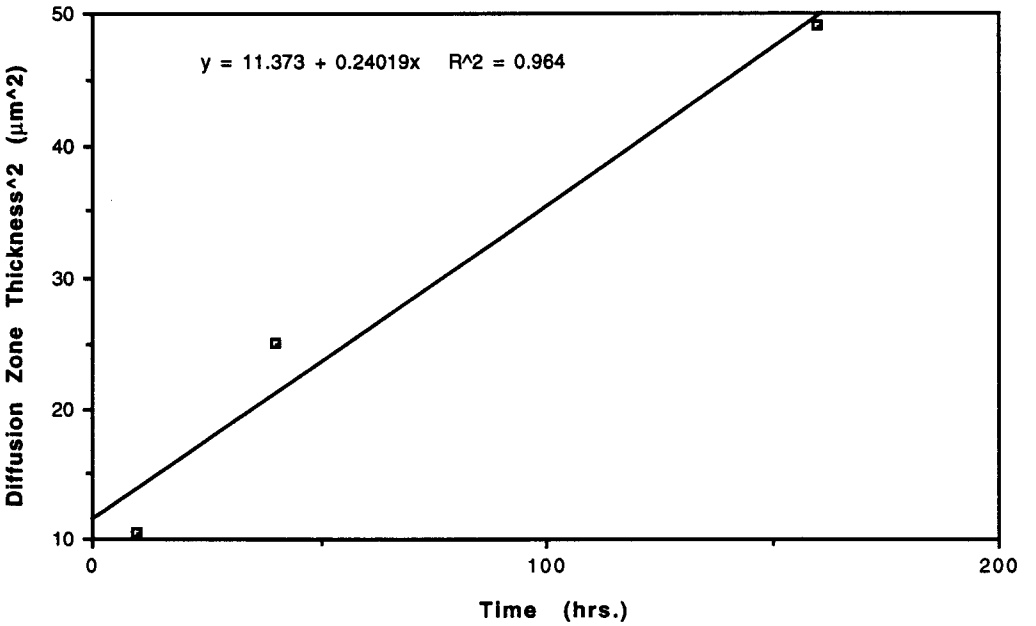

Figure A11. Diffusion Zone Thickness squared versus Time, Ta>Ir, 1300°C.

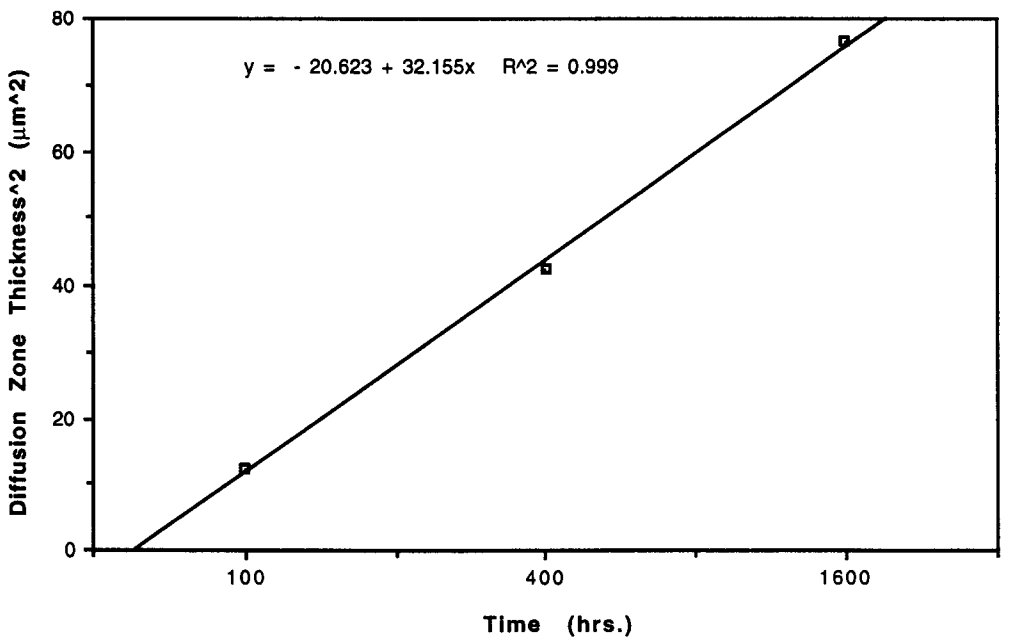

Figure A12. Diffusion Zone Thickness squared versus Time, Ta>Ir, 1150°C.

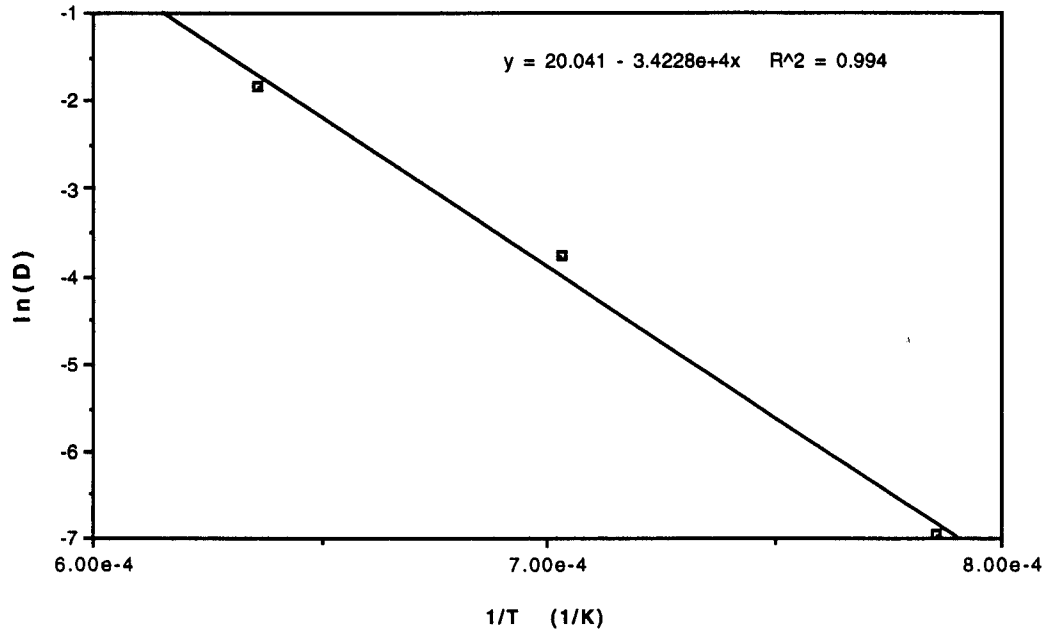

Figure A13. Natural Log of Diffusivity versus Reciprocal Absolute Temperature, Mo>Ir.

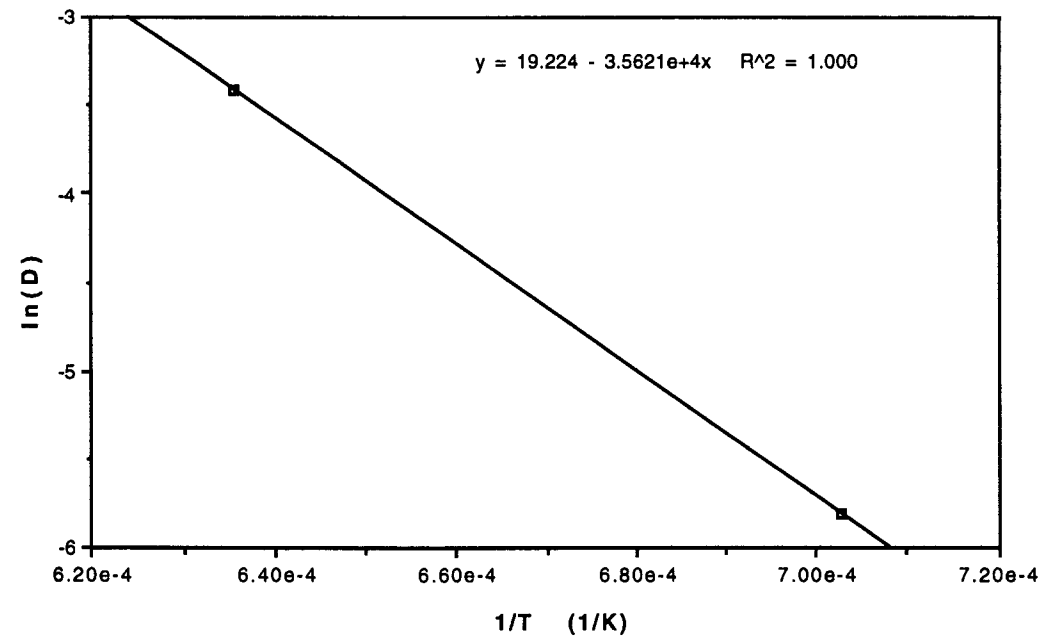

Figure A14. Natural Log of Diffusivity versus Reciprocal Absolute Temperature, Ir>Mo.

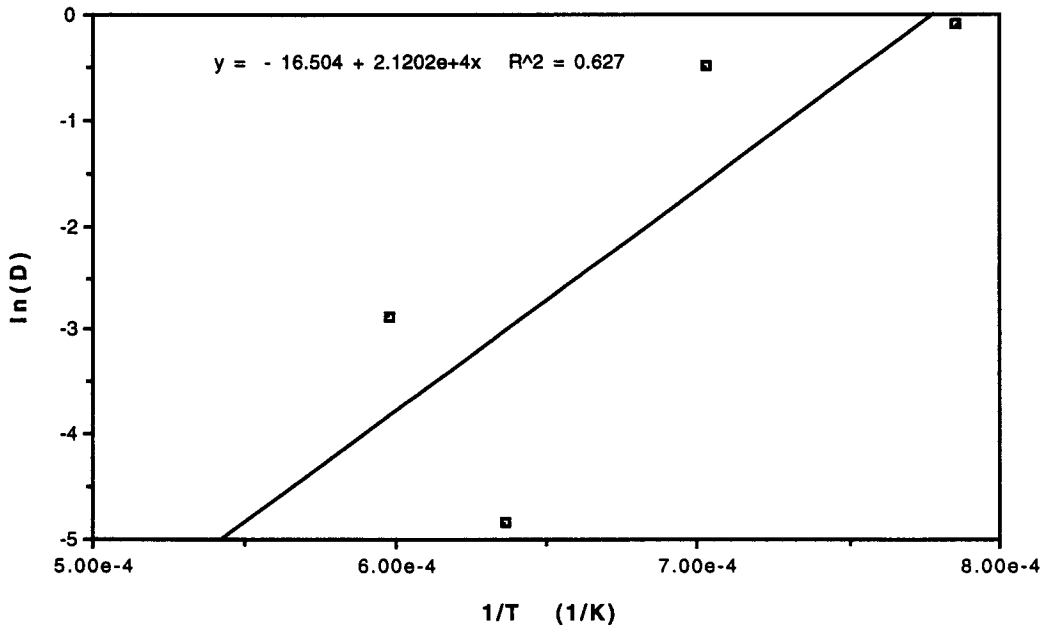

Figure A15. Natural Log of Diffusivity versus Reciprocal Absolute Temperature, Ir>T-111.

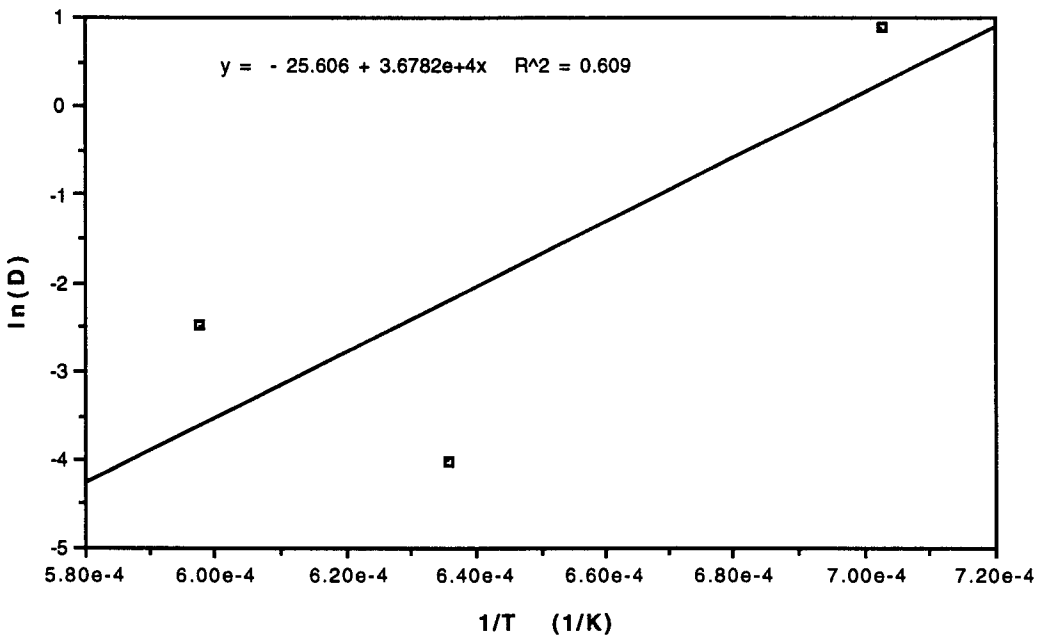

Figure A16. Natural Log of Diffusivity versus Reciprocal Absolute Temperature, Ta>Ir.

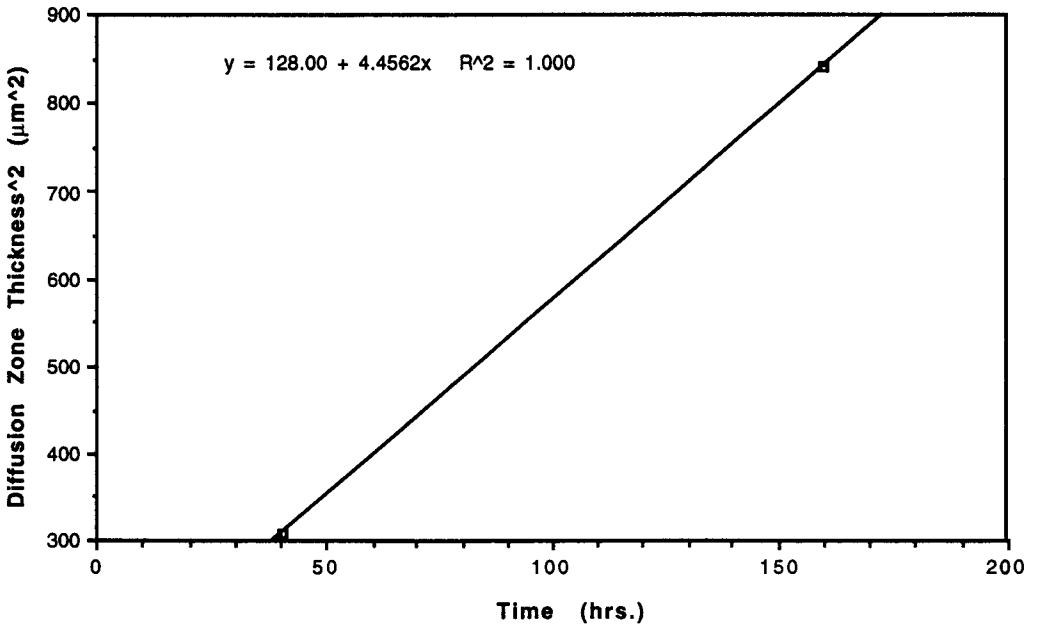

Figure A17. Combined Diffusion Zone Thickness squared versus Time, Mo/Ir, 1300°C.

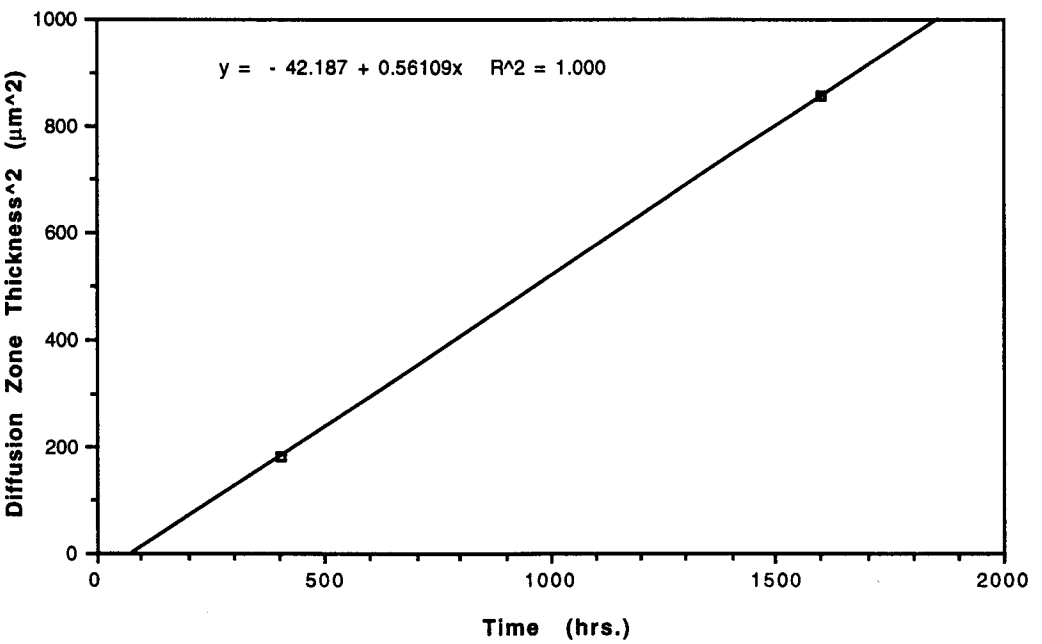

Figure A18. Combined Diffusion Zone Thickness squared versus Time, Mo/Ir, 1150°C.

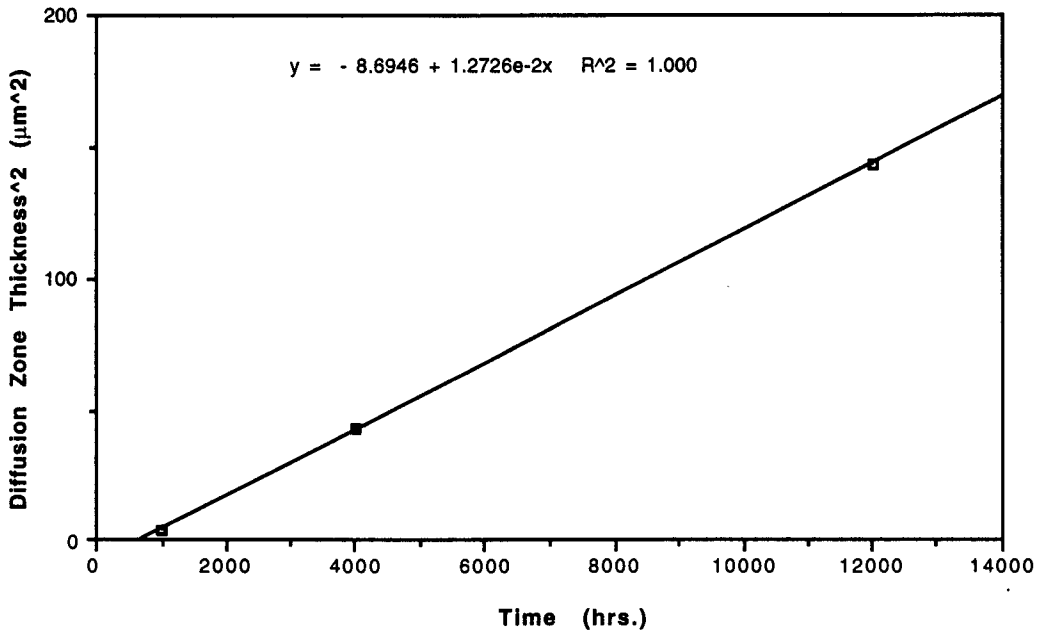

Figure A19. Combined Diffusion Zone Thickness squared versus Time, Mo/Ir, 1000°C.

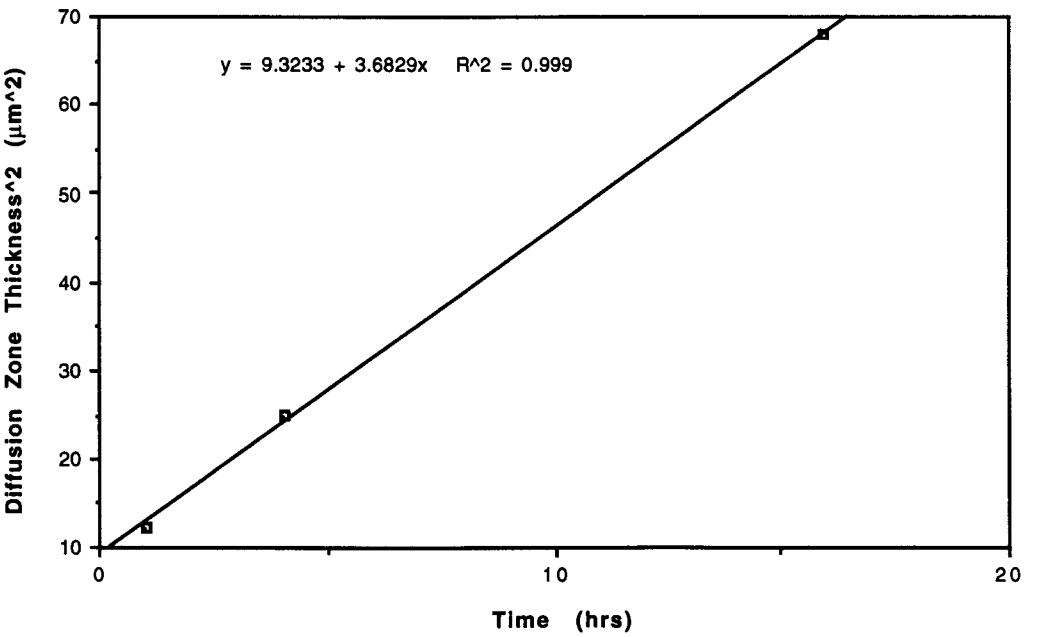

Figure A20. Combined Diffusion Zone Thickness squared versus Time, Ir/T-111, 1400°C.

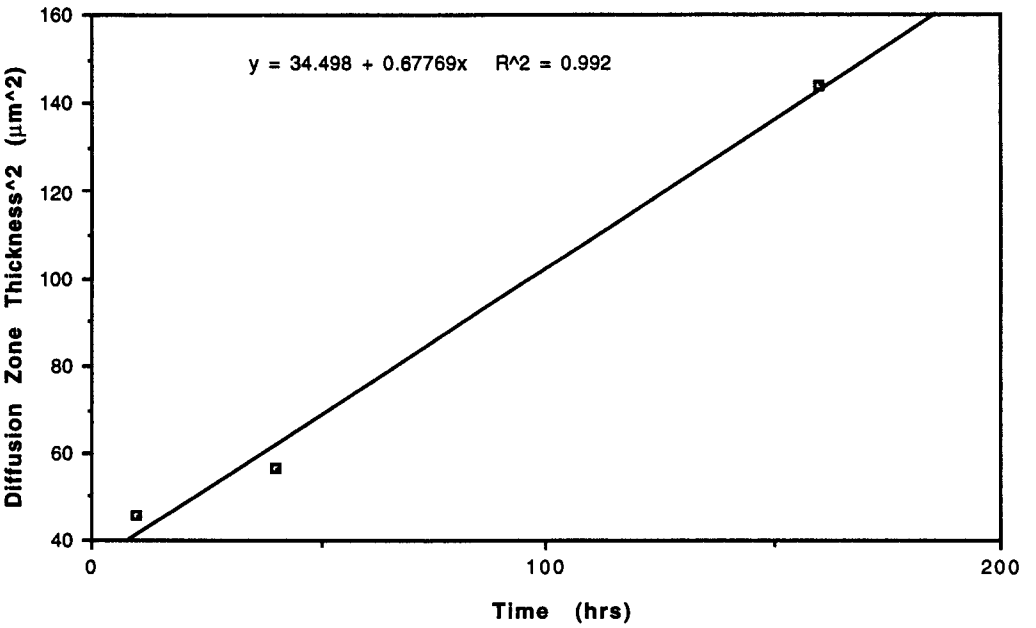

Figure A21. Combined Diffusion Zone Thickness squared versus Time, Ir/T-111, 1300°C.

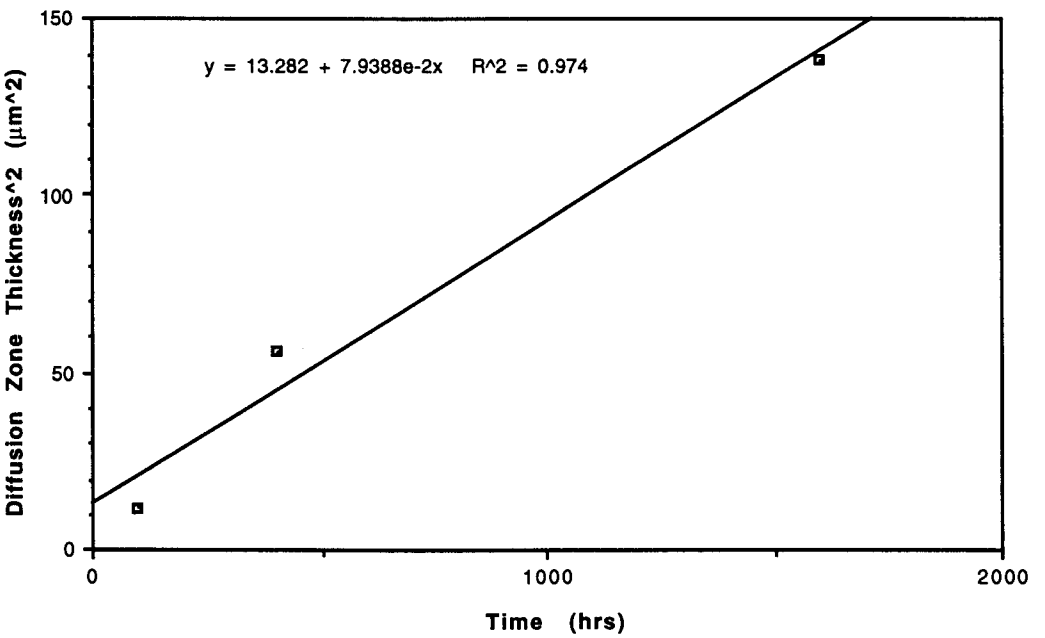

Figure A22. Combined Diffusion Zone Thickness squared versus Time, Ir/T-111, 1150°C.

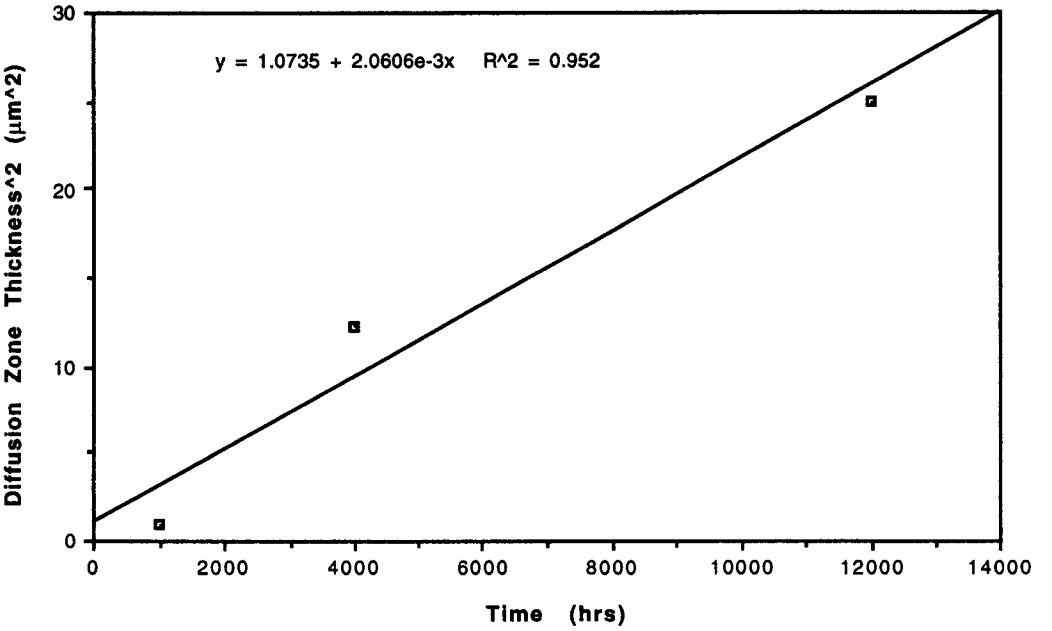

Figure A23. Combined Diffusion Zone Thickness squared versus Time, Ir/T-111, 1000°C.

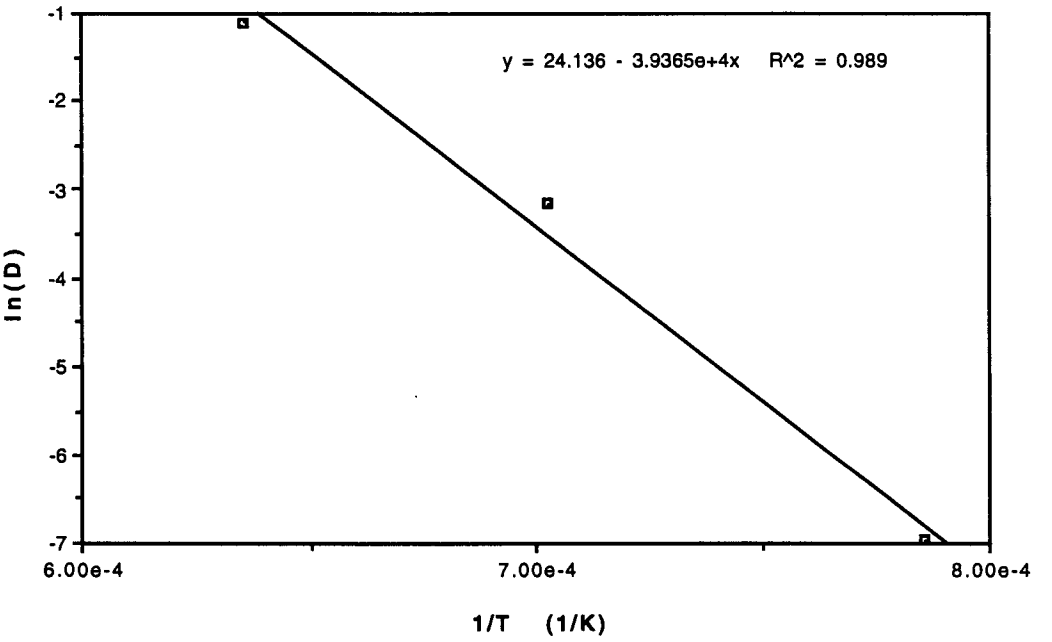

Figure A24. Natural Log of Diffusivity versus Reciprocal Absolute Temperature for Combined Diffusion Zone Thickness, Mo/Ir.

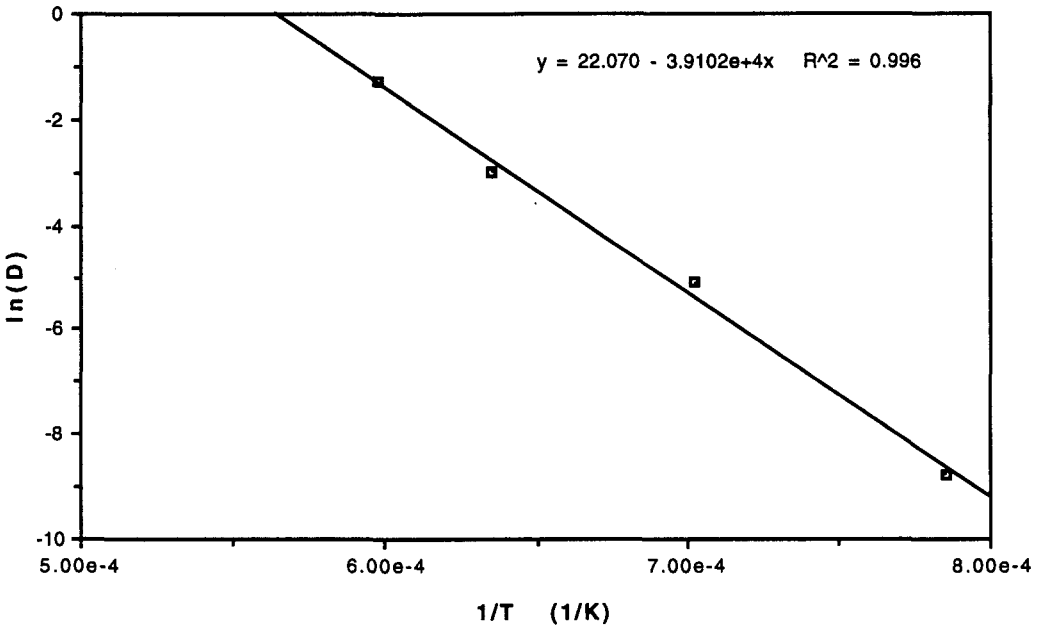

Figure A25. Natural Log of Diffusivity versus Reciprocal Absolute Temperature for Combined Diffusion Zone Thickness, Ir/T-111.